Energy Storage Materials 2 (2016) 35–62

Contents lists available at ScienceDirect

Energy Storage Materials

journal homepage: www.elsevier.com/locate/ensm

Metal organic frameworks for energy storage and conversion

Yang Zhao [1], Zhongxin Song [1], Xia Li, Qian Sun, Niancai Cheng, Stephen Lawes, Xueliang Sun *

Department of Mechanical and Materials Engineering, University of Western Ontario, London, Ontario, Canada N6A 5B9

ARTICLE INFO

Article history:
Received 8 September 2015
Received in revised form
13 November 2015
Accepted 14 November 2015
Available online 28 November 2015

Keywords:
Metal–organic frameworks
Energy storage and conversion
Fuel cell
Lithium ion batteries
Supercapacitors

ABSTRACT

Metal–organic frameworks (MOFs), a novel type of porous crystalline materials, have attracted increasing attention in clean energy applications due to their high surface area, permanent porosity, and controllable structures. MOFs are excellent precursors for the design and fabrication of nanostructured porous carbons and metal oxides, especially for hierarchical nanostructures. In this review, the recent development and understanding of MOFs and MOF-derived nanomaterials in the applications of fuel cells, batteries (e.g. lithium-ion, lithium–sulfur, and lithium–air batteries), and supercapacitors are summarized in detail. In particular, we focus on the design and fabrication of the morphology of nanomaterials derived from MOFs and the significant impact of structure on the electrochemical performance in clean energy applications. Finally, we also present the future trends, prospects, and possible obstacles of the development of advanced MOFs and MOF-derived nanomaterials for more promising and large-scale commercial applications of clean energy.

Contents

* Corresponding author.
E-mail address: xsun@eng.uwo.ca (X. Sun).
[1] Yang Zhao and Zhongxin Song contribute equally to this work.

http://dx.doi.org/10.1016/j.ensm.2015.11.005
2405-8297/

1. Introduction

1.1. Metal organic frameworks

Metal–organic frameworks (MOFs) are crystalline materials composed of metal ions (or metal clusters) and organic linkers [1–5]. As a novel class of porous materials, MOFs have attracted great attention in recent years owing to their high surface area and permanent porosity.

Fig. 1 shows the structures of some reported MOFs. As shown in the figure, MOFs are made by linking inorganic and organic units via strong chemical bonds. The organic units are divalent or polyvalent organic carboxylates, which when linking to metal-containing units (e.g. Zn^{2+}, Co^{2+}, Cu^{2+}, Mg^{2+}, Ni^{2+}, Al^{3+}), can yield architecturally three-dimensional structures with well-defined pore size distributions. The surface area of MOFs typically ranges from 1000 to 10,000 m^2/g, and pore size can be tuned as large as 9.8 nm by altering the organic and metal-containing units [6–9]. As O'Keeffe previously reported, the same metal clusters could be connected by ditopic carboxylate linkers with different lengths to produce a variety of MOFs materials with the same network topology (Fig. 1b) [10]. The variety of constituents' geometry, size, and functionality has led to more than 20,000 different MOFs being reported and studied within the past few decades [2]. Transition metals (e.g. Zn, Co, Cu, Fe, Ni), alkaline earth elements (e.g. Sr, Ba), p-block elements (e.g. In, Ga), actinides (e.g. U, Th), and even mixed metals have been used for the synthesis of MOFs [11–15]. For example, MOF-5 is commonly based on nets of linked Zn_4O tetrahedrons via 1,4-benzenedicarboxylate (1,4-BDC) ligands, resulting in a three-dimensional cubic network structure with interconnected pores diameter of 12 Å. Moreover, simply changing the metal units from Zn_4O to Cr_3O results in an obvious change in structure from MOF-5 to MIL-101, which contains large cages with the diameter of ~3 nm (Fig. 1) [16]. Since they are comprised of two main components, MOFs with desired structures can be designed by careful selection of metal centers and different organic ligands [17].

1.2. Nucleation and growth mechanism of MOFs

The most prevailing synthesis methods for MOFs are hydrothermal and solvothermal approaches (Fig. 2) [18], which have reaction times from several hours to days. In a typical solution-based MOFs forming process, a nanoporous material can be formed through a process of nucleation and spreading, and then multiple nucleation aggregate with surface adsorbed organic molecules into an inorganic–organic crystal. To produce controllable nanoscale MOFs crystals and shorten the synthesis time, some alternative synthesis approaches have been attempted, such as microwave-assisted [19–21], sonochemical [22], electrochemical [23], and mechanochemical methods [24].

A key structural feature of MOFs is their high porosity as well as high surface area, which plays a crucial role in their functional properties. Therefore, understanding the molecular forming mechanism of MOFs has been a widely researched topic [25–27]. By in situ observing the MOFs surface features in the process of nucleation and spreading, Moh and co-workers [26] revealed the forming process of Zeolitic Imidazolate Framework-8 (ZIF-8) in 2011. As Fig. 3(I) shows, the nanoporous ZIF-8 occurs through a process of surface nucleation and spreading of successive metastable unenclosed sub-steps in a correlated manner, eventually forming stable surface steps of the enclosed framework structure. After that, Zhou et al. revealed the formation mechanism of MOF-5 [$Zn_4O(C_8H_4O_4)_3$] crystals. It is demonstrated that in the earliest stage, Zn^{2+} and $C_8H_4O_4$ molecules combined with each other and forming crystalline nanoplates with diameter of 5–10 nm. With the assistance of 1,4-BDC molecules, the nanoplates aggregate fast from surface adsorbed organic molecules into layered inorganic–organic microplates. With an increase in reaction time to 6 h or longer, all the microplates further joined together to form loosely

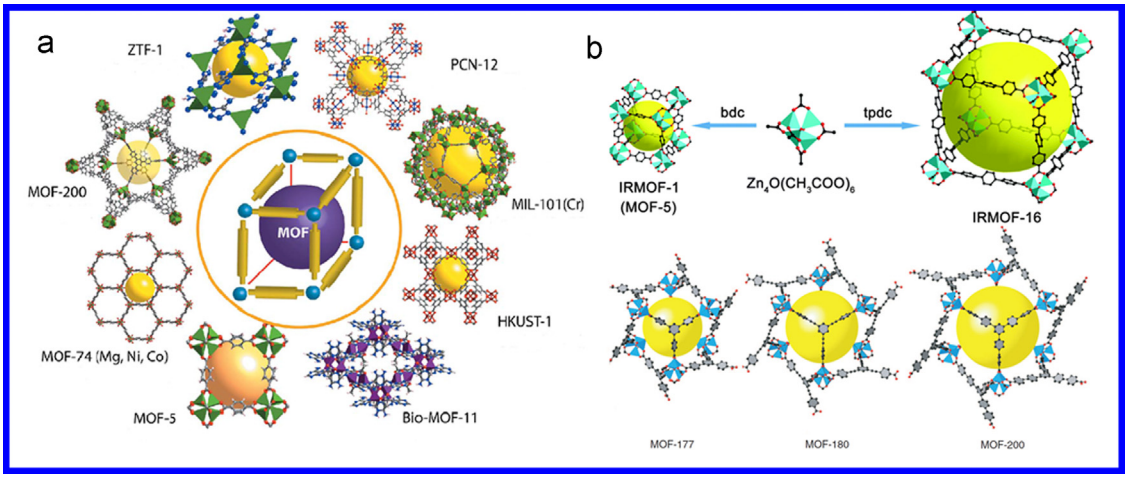

Fig. 1. Schematic representation of reported MOFs structures [3,16].

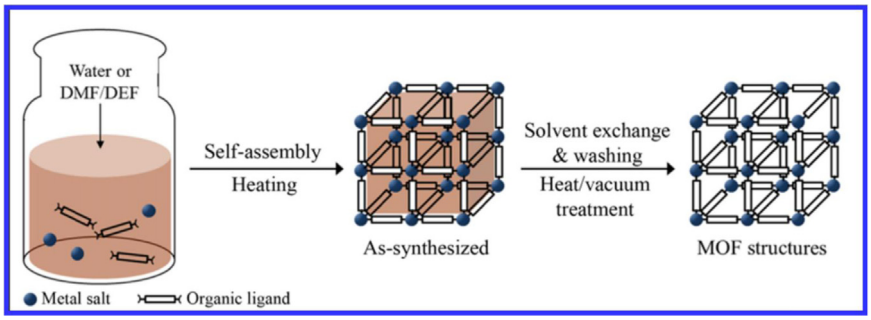

Fig. 2. Conventional solvothermal synthesis of MOFs structures [18].

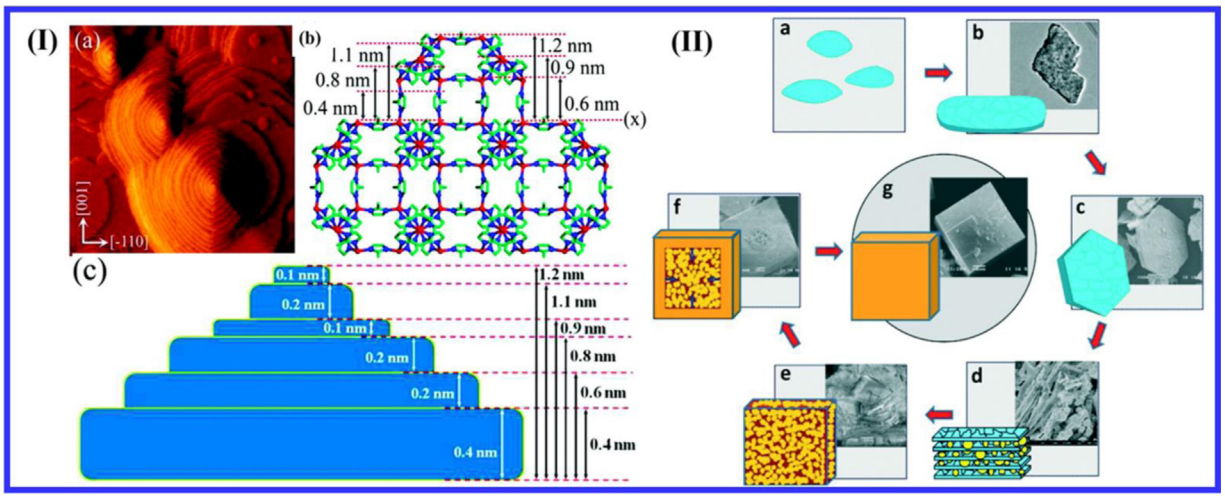

Fig. 3. Schematic drawing of the proposed formation mechanism for (I) ZIF-8 and (II) MOF-5 cubes [26,27].

stacked layered particles approximately 80–200 μm in diameter and about 20 μm in thickness (Fig. 3(II)f), followed by surface recrystallization and reversed crystal growth, leading to cubic single crystals as the final product. The proposed formation mechanism of MOF-5 is elucidated from (a) to (g) in Fig. 3(II) [27].

1.3. Fabrication of MOF-derived nanostructured materials

Due to the controllable micro- and meso-porous nanostructures, MOFs materials have been considered as one of the most promising candidates for the applications in energy storage and conversion. Apart from pure MOFs, some MOF-derived materials with highly controlled nanostrucutres have received increased attention for electrochemical applications in recent years. By the fact that MOFs can be converted to the desired products through one-step calcination process, MOFs have been successfully applied to develop nanostructured carbon, metal oxide as well as metal oxide/carbon composites.

1.3.1. MOF-derived nanostructured carbon

The large content of carbon-based organic linkers in MOFs facilitates the design of nanostructured carbon using MOFs as sacrificial materials [28,29]. Because MOFs inherently consist of metallic species which are an integral part of the whole structure, it is essential to remove these metallic species to get high surface area carbon. In 2012, Yamauchi et al. first reported direct carbonization of Al-porous coordination polymers to fabricate carbon [30]. The obtained nanoporous carbon possessed an extremely high surface area over 5000 $m^2 g^{-1}$ and a large pore volume of 4.3 $cm^3 g^{-1}$. It was also revealed that the carbonization temperature was critical to realize such high surface area and pore volume.

Another method for preparing nanostructured carbon with high porosity can be achieved by infiltrating a secondary carbon source into the cavities of MOFs hard-templates [31–33]. Carbonization of MOFs with secondary precursor commonly results in high surface area carbon. In 2011, Xu and co-workers reported using pristine ZIF-8 to obtain the high surface area carbon, furfuryl alcohol was introduced into ZIF-8 as a secondary carbon source, which gave unexpectedly high surface area of 3405 $m^2 g^{-1}$ and a total pore volume of 2.58 $cm^3 g^{-1}$ [34]. Besides furfuryl, some other carbon-based organics like glycerol, carbon tetrachloride, ethylenediamine, and phenolic resin have been reported for using as secondary carbon sources in MOFs cavities for producing nanostructured carbon.

1.3.2. MOF-derived nanostructured metal oxide

Because of the inherent structures of MOFs, which are made up of metal centers coordinated with organic complexes, controlled heating in various environments can produce MOF-derived metal oxide with unique structures. A successful derivation of Fe_2O_3 with spindle like mesoporous structures from MIL-88 (Fe) has been reported. Microstructure analysis showed that the product was highly porous and consisted of uniform nanoparticles with a size of about 20 nm [35]. In addition, another advantage of using MOFs as template is that carbon–metal/metal oxide hybrids can be simply produced [29,31]. In 2011, Liu and co-workers reported using Co-MOFs as template to produce Co–N_x–C nanoparticles. It was revealed that during the thermal carbonization process, the organic linkers would be converted to carbon while maintaining the porous framework, with the formation of Co–N_x units uniformly distributed in the carbon framework. The porous carbon

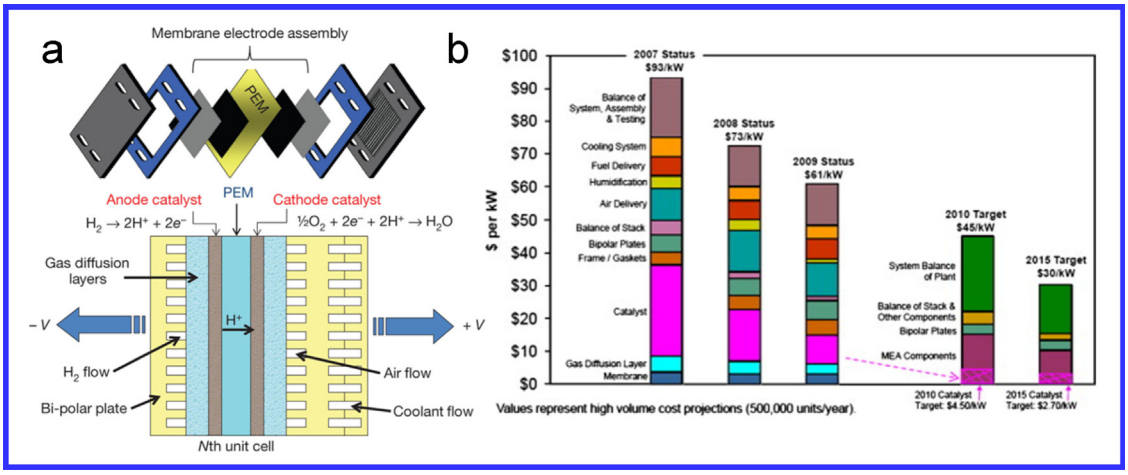

Fig. 4. (a) Typical PEMFC operation [38]. (b) Status and DOE targets of fuel cell costs [42].

framework with Co–N_x sites, which have been considered as an effective electrochemical catalyst for oxygen reduction [36].

2. MOFs for fuel cell applications

2.1. Introduction, challenges, and objectives of fuel cells

A fuel cell is an electrochemical conversion device that has a continuous supply of fuel, such as hydrogen, natural gas, or methanol, and oxidant such as oxygen, air, or hydrogen peroxide. Each fuel cell consists of an anode, a cathode, and electrolyte which allows ions to move between the two sides of the fuel cell [37]. Fig. 4a illustrates the basic operational processes within a typical polymer electrolyte membrane fuel cell (PEMFC) [38]. Hydrogen (H_2) as a fuel is delivered to the anode where it can be oxidized by anodic catalyst producing protons and electrons. The protons pass through the electrolyte and reach to the cathode side, while the electrons travel to an external circuit with supplying a current. At the cathode, with the assistant of catalyst, oxygen (O_2) combine with protons and electrons producing water and releasing some heat.

The clean point of operation emissions, fast refueling times and excellent energy density render PEMFCs promising for a variety of applications. Hydrogen fueled PEMFCs vehicles would allow us to significantly cut back on the over five billion tons of greenhouse gas emissions (CO_2) produced by automobiles each year [39]. However, there are two device level limitations that currently limit the attractiveness of PEMFCs in the automotive market: high cost and insufficient durability. The key technical U.S. Department Of Energy (DOE) targets are to develop a fuel cell system for portable power (< 250 W) with an energy density of 900 W h L^{-1} by 2015, and achieve a direct hydrogen fuel cell power system for transportation with a peak-efficiency of 60%, 5000 h durability and a mass-produced cost of \$30 kW^{-1} by 2017 [40]. Among the various components, the platinum (Pt)-based electrocatalysts required at each electrode to facilitate the electrochemical reactions are the biggest contributors to PEMFCs cost and durability issues [41]. The Pt-based electrocatalysts are estimated to contribute almost 50% of the cost of membrane electrode assembly (MEA) component (Fig. 4b) [42]. However, Pt is currently the most efficient electrocatalyst in practical PEMFCs due to its outstanding catalytic, electrical, and corrosion-resistance properties [43]. Therefore, It is highly desirable to find efficient and inexpensive alternatives to Pt-based catalysts for PEMFCs [44,45].

MOFs, as described previously, could be tailored to have a high surface area and a regular porous structure. By tuning their structures through carefully selecting metal clusters and multifunctional linkers, the desired MOFs product can be designed with rich metal (e.g. transition metal: Co, Fe, Cu, etc.), nitrogen, carbon sites and that would be beneficial for fabricating good electrochemical catalysts. In the field of fuel cells, MOFs and MOF-derived nanostructured materials working as efficient electrochemical catalyst have been widely reported in recent years. In this review, the great designable of MOFs enables their multiple applications on fuel cell will be discussed.

2.2. MOFs as electrocatalysts

MOFs consist of metal clusters, which can be comprised of electrochemically active metals. Thus, by rationally designing the composition of frameworks and taking advantages of the adaptive encapsulation properties of MOFs, it is easy to synthesize electrochemically functional MOFs with catalytic properties. The first example for the utilization of MOFs as electrocatalysts for oxygen reduction reaction (ORR) was demonstrated by Lanqun Mao's group [46]. Two kinds of Cu-based MOFs were synthesized, [copper (II) benzene-1,3,5-tricarboxylate] and [copper (II)-2,2′-bipyridinebenzene-1,3,5-tricarboxylate]. The synthetic [copper (II)-2,2′-bipyridinebenzene-1,3,5-tricarboxylate] MOFs was found to exhibit an excellent and stable electrocatalytic activity towards $4e^-$ reduction of O_2. Based on the excellent catalytic performance of Cu-MOFs, some graphene and Cu-MOFs composites have been researched to overcome the poor electron-conduction properties of Cu-MOFs and further improve the catalytic activity and stability. In 2013, Maryam Jahan and co-workers developed a graphene oxide (GO)-incorporated copper-centered MOFs composite (GO-Cu-MOFs) (Fig. 5(II)), which exhibited good catalytic activity for ORR, oxygen evolution reaction (OER), and hydrogen evolution reaction (HER) [47]. With the excellent tri-functional catalytic activity, GO-Cu-MOFs composites exhibited quite little overpotentials and high current density for all three electrocatalytic reactions and showed excellent stability in acid media. Particularly, for the oxygen reduction, there is a significant enhancement of cathodic peak at 0.29 V (vs. RHE) in O_2-saturated H_2SO_4 for (GO 8 wt%)-Cu-MOFs which is better than pure Cu-MOFs at 0.16 V (vs. RHE), which suggested that the incorporation of GO into the MOFs improves the electrocatalytical behavior. In terms of power density, the maximum power density of 110.5 mW cm^{-2} was achieved for (GO 8 wt%)-Cu-MOFs which is 76% that of Pt/C. All of these good electrocatalytic performance combined with its low cost and

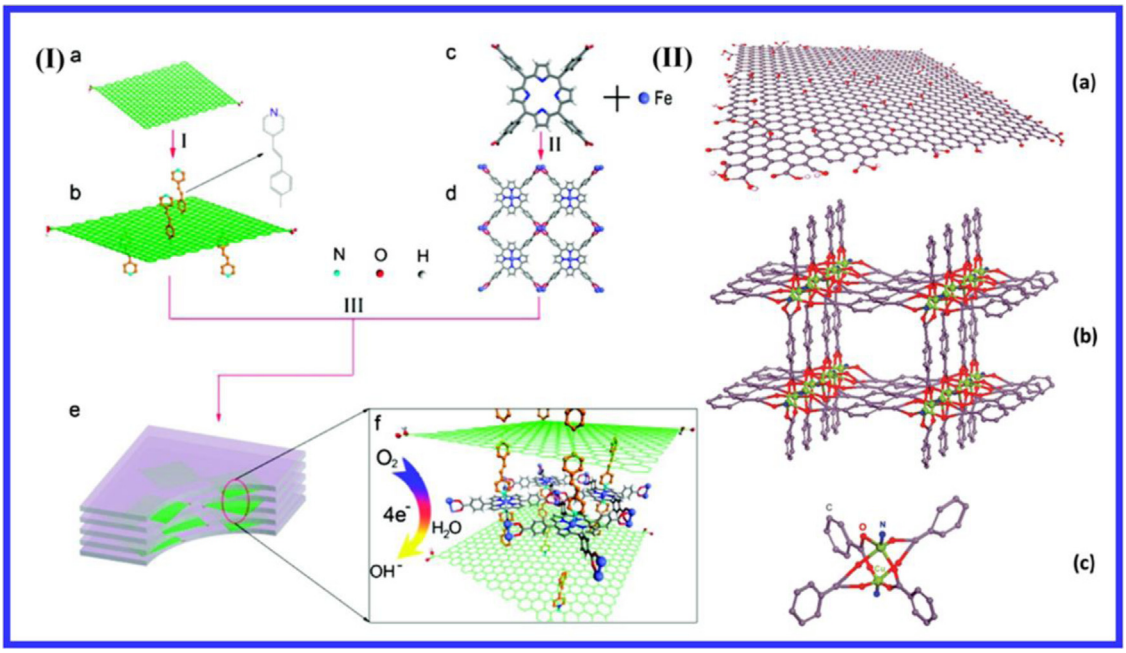

Fig. 5. Synthetic routes to produce (I) (r-GO-FeP)n-MOFs. (II) Schematic of the chemical structures of (a) GO, (b) GO-Cu-MOFs composites, (c) Cu-MOFs [47,48].

facile synthesis makes GO-Cu-MOFs hybrids a promising alternative to Pt catalysts in fuel cell applications.

Except for the Cu-based MOFs, graphene-Fe-MOFs were synthesized and employed as ORR catalyst by Kian Ping Loh group in 2012 [48]. The reduced GO (r-GO) sheets that are functionalized on both sides of the plane with pyridine ligands; these functional r-GO as struts to link metalloporphyrin (FeP) nodes to form the r-GO-MOFs hybrids. It was demonstrated that the weight percentage of functionalized r-GO added to the framework plays a great role in the structure and electrochemical property of the (r-GO-FeP) MOFs, due to functionalized r-GO can influence the crystallization process of MOFs. When an appropriate amount of 50 wt% r-GO is added, $(r\text{-}GO\text{-}50wt\%\ \text{-}FeP)_n$ MOFs exhibit the excellent ORR performance with the onset-potential of -0.23 V (vs. Ag/AgCl). The presence of r-GO act synergistically with FeP catalysts to afford facile 4-electron ORR pathway and this kind of MOFs composite also possessed the reduced methanol crossover effects compared to Pt catalyst (Fig. 5(I)).

2.3. MOF-derived carbon as metal-free electrocatalysts

MOF-derived nanostructured carbon materials work as electrocatalysts in fuel cell have been widely investigated by many researchers [49,50]. In 2014, the highly graphitic nitrogen-doped porous carbons (NGPCs) derived from ZIF-8 as efficient electrocatalysts for ORR was reported by Hong et al. In a facile carbonization process, ZIF-8 worked as both the carbon and nitrogen sources and resulted in the NGPCs product not only retain the morphology of parent MOFs but also possess rich nitrogen, high surface area and well-conducting network (Fig. 6). It was assumed that the carbonization time and temperature play a critical role in the electrochemical property of NGPCs. For 1000 °C and 10 h carbonization, the resultant NGPCs-1000-10 exhibit good ORR performance with high current density of 4.3 mA cm^{-2} and oxygen reaction onset-potential (the highest potentials for cathodic reactions at which a reaction product is formed) of −0.02 V (vs. Ag/AgCl) which is only 40 mV negatively shifted compared to that of Pt/C. The outstanding electrocatalytic activity of this true metal-free catalyst is attributed to the synergetic contributions of abundant graphitic-N active sites, high surface area and the high degree of graphitization. In order to get the in situ nitrogen-doped porous carbon with huge surface area and narrow pore size distribution, a second carbon source was suggested to be introduced into MOFs framework [51]. Using glucose as a secondary carbon precursor, which was infiltrated into the pores of MOFs precursor zinc-benzimidazole [ZIF-7], after carbonization at 950 °C for 5 h, the proposed nitrogen-doped porous carbon was synthesized. Importantly, the addition of carbon source glucose can not only improve the graphitization degree of resultants, but also favors of removal Zn metal and Zn compound impurities from ZIF-7, which makes a real metal-free electrocatalyst for fuel cells. Compared with the electrocatalytic performance of ZIF-7-derived carbon, glucose-derived carbon, ZIF-7/glucose-derived carbon made by mixing ZIF-7 and glucose precursors in liquid phase exhibit the best ORR activity with the onset-potential of 0.86 V (vs. RHE) and nearly four-electron selectivity (the electron transfer number is 3.68 at 0.3 V) in O_2-saturated 0.1 M KOH, which is much close to the commercial Pt/C. Besides the ORR activity, this kind of nitrogen-doped carbon also have better stability and methanol tolerance than the commercial Pt/C catalyst. It was revealed that nitrogen-containing MOFs/carbon source composites can be used as precursor to make nitrogen-doped porous carbon as efficient electrocatalysts for ORR, owing to their structures with graphene-like morphology, high BET specific surface area, and high porosity.

In order to develop more active sites on the MOF-derived nanostructured carbon, some heteroatoms (e.g. N, S, P) can be designed doping on the MOFs-carbon materials, which will make contributions to their electrocatalytic activity. MOF-5 as template by encapsulated with urea and dimethyl sulfoxide (DMSO) after carbonized at 900 °C for 5 h, the nitrogen and sulfur co-doped nanoporous carbon (N, S-MOFs-C) can be synthesized, in which MOFs, urea and DMSO act as template and carbon source, nitrogen and sulfur source respectively [52,53]. It was revealed that the heteroatom-co-doped N, S-MOFs-C as electrocatalyst could reduce oxygen at the relatively high onset-potential of −0.005 V (vs. Ag/AgCl) in O_2-saturated 0.1 M KOH solution and with a 3.8 electron transfer pathway, which is owing to the synergetic effect between active sites of heteroatoms N, S and C ($C\text{–}N_x$, $C\text{–}S_x$). In terms of long-term durability and methanol resistance ability, N, S-MOFs-C

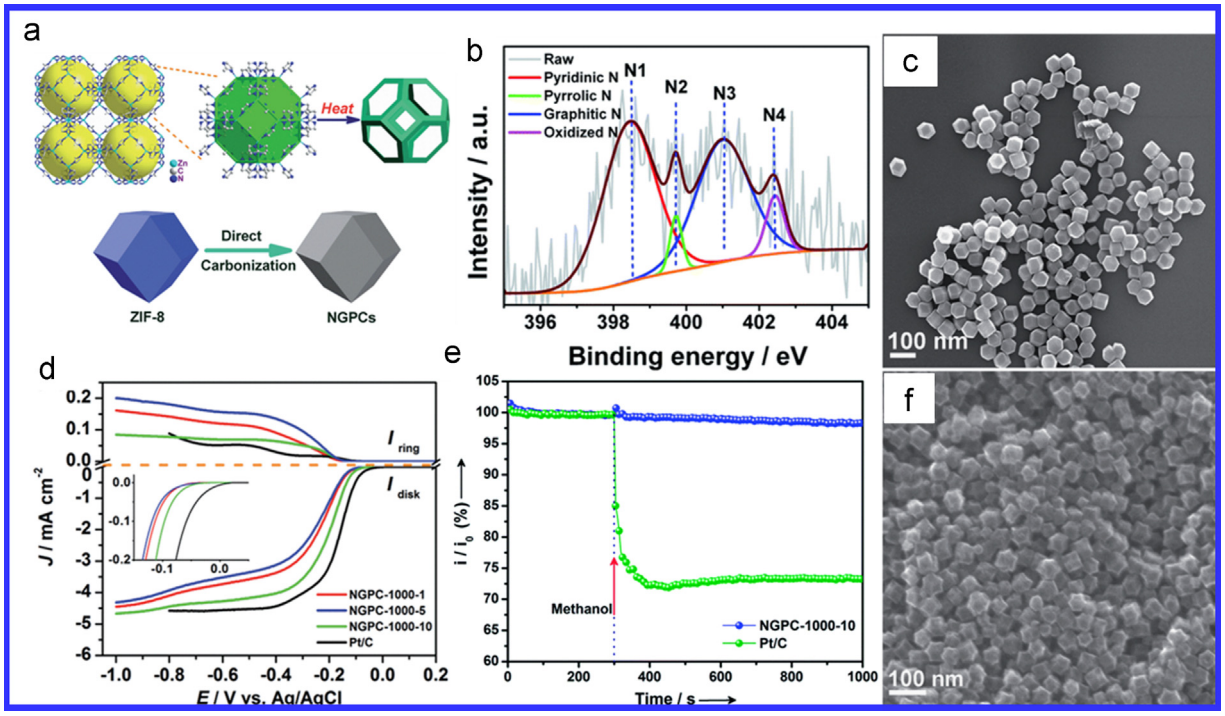

Fig. 6. (a) Schematic illustration of synthesis ZIF-8 derived nitrogen-doped porous carbon (NGPC). (b) XPS N1s spectrum of NGPC-1000-10. (c) SEM of mono-disperse ZIF-8 nanopolyhedra. (d) Linear sweep voltammograms of NGPCs and Pt/C in O_2-saturated 0.1 M KOH solution at 1600 rpm with a scan rate of 5 mV s^{-1}. (e) Current–time (*i*–*t*) chronoamperometric responses at −0.4 V in O_2-saturated 0.1 M KOH on NGPC and Pt/C electrodes (1600 rpm) followed by the introduction of methanol (3 M) at 300 s. (f) SEM images of NGPC-1000-10 [49].

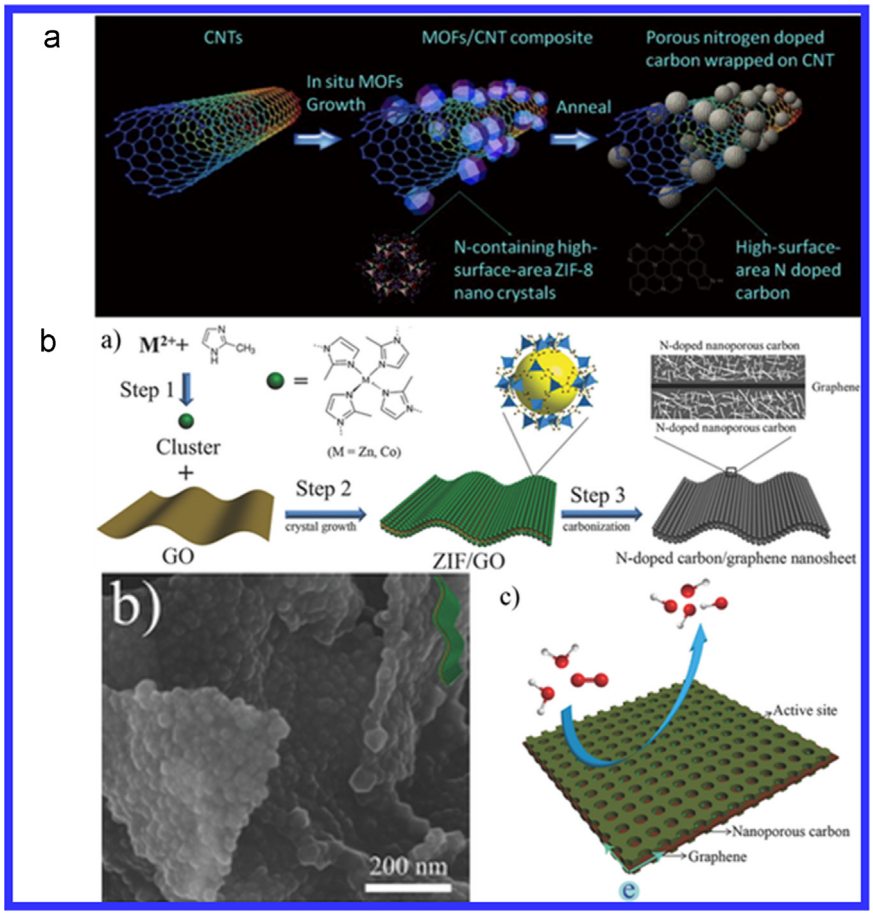

Fig. 7. (a) The strategy to develop high-surface-area N-doped carbon from ZIF-8/CNTs composites. (b) The schematic synthesis of N-doped nanoporous carbon/graphene nano-sandwiches [55,56].

exhibit good selectivity for ORR and outperforms the commercial Pt/C in the presence of methanol.

By fabricating the MOFs precursors with nitrogen containing ligands, the self-nitrogen doped nanocarbon can be arrived after MOFs carbonization. Generally, it should be noted that the incorporation of MOF-derived nanocarbon into the 1-D carbon nanotubes or 2-D graphene can significantly enhance the surface polarity, electric conductivity, and electron-donor tendency of the nanocarbon, resulting in an enhanced performance in the applications especially in fuel cells electrocatalyst. In 2014, Shim and co-workers described a method for homogeneously coating MOFs on the outer surface of CNTs [54]. By simply changing the concentrations of the MOFs in MOFs/CNTs composites, MOFs-based continuous layers can be formed on CNTs surface.

Furthermore, Zhu's group synthesized a novel ORR electrocatalyst based on N-containing nanocarbon produced from an in-situ grown ZIF-8/CNTs composite, the schematic is shown in Fig. 7 (a) [55]. This strategy delivers high-performance electrocatalysts by taking advantage of the merits of these interacting materials. The CNTs were applied as a high conductivity skeleton in the final electrocatalyst with N-nanocarbon decoration leading to abundant catalytic sites on the CNTs skeleton. The excellent affinity between the continuous thin N-nanocarbon layer and the CNTs skeleton contribute to high ORR electrocatalytic activity and superior stability in alkaline electrolyte. The incorporation of an ultrathin layer of nanoporous carbon, in particular nitrogen-doped nanoporous carbon, on graphene surface has been investigated as ORR electrocatalyst by Wang's group [56]. It was demonstrated that the combination of nanoporous carbon thin layer on the graphene leading to the formation of a N-nanocarbon/graphene/N-nanocarbon sandwich-like structure (as shown in Fig. 7(b)) with functionalization, high specific surface area and good electrical conductivity, all of these make contributions to fast mass transport and electron transfer required by ORR. During an oxygen reduction process, graphene acts as a conductive layer to accelerate the electron transfer in the carbon matrix and readily reach to the catalytic layer smoothly. The high specific surface area and nanoporous structure of N-nanocarbon/graphene nanosheets facilitate the fast transport of reactants to reach the active sites and removal of corresponding products due to the short transport pathway.

2.4. MOFs as precursors for non-precious metal eletrocatalysts

Accordingly, extensive efforts have been devoted to develop highly efficient, economical, and earth-abundant catalysts for ORR to replace Pt-based noble metal catalysts. Among them, transition metal–nitrogen–carbon (M–N–C) materials, especially for Co–N–C or Fe–N–C, have been a major focus of research and development, due to their excellent electrocatalytic activity. It is worth noting that N-doped metal species @ carbon hybrids derived from different MOFs precursors with the advances of homogeneous distributed active sites and nanoporous structures have attracted wide attentions. Li and co-workers demonstrated the application of Co-based MOFs (ZIF-67) as precursor for fabricating the nanoporous Co–N_x–C hybrid which can be used as an efficient ORR catalyst in both alkaline and acidic electrolyte (as shown in Fig. 8). In their work, by optimizing the pyrolysis temperature and acid leaching process, the as-prepared Co–N_x–C hybrid with rich porosity and ordered graphitic structure exhibited outstanding ORR activity and good stability, which suggesting that the ideal structures of highly dispersed Co–N_x active sites in the nanoporous conductive system are essentials to drive for ORR catalyst with high performance [57]. Except for these features, the particle size of precursor ZIF-67 was found also has an intense effect on the catalytic activity [58]. Comparison between the ZIF-67-derived catalysts, it was revealed that the ORR activity and stability increases as the size of the precursor decreases from several micrometers to 300 nm, and Co–N_x–C polyhedra prepared from the smallest ZIF-67 particles exhibit the highest ORR activity, which is due to the smaller particle could provide more active sites and easily access to catalytic centers and thus promote a faster mass and electron transfer process.

Besides Co-based MOFs, some functionalized MOFs structures composed of Fe species can also be used as excellent precursors to fabricate non-precious metal electrocatalyst for fuel cell application. It was reported that the nanoscale Fe-based MOFs [MIL-88B NH_3] with controllable size and shape can be used as the pyrolytic precursor to develop non-precious metal catalyst (Fig. 9) [59]. Pyrolysis at 900 °C, [MIL-88B NH_3] could be converted to Fe and N co-doped nanocarbon (Fe/FeN/C). As the high performance ORR catalyst, Fe/FeN/C exhibits much more positive onset potential of 1.03 V (vs. RHE) than that of Pt/C (1.01 V). Furthermore, the diffusion-limited current density of Fe/FeN/C catalyst is considerably 1.2 times higher than that of Pt/C, which represents the

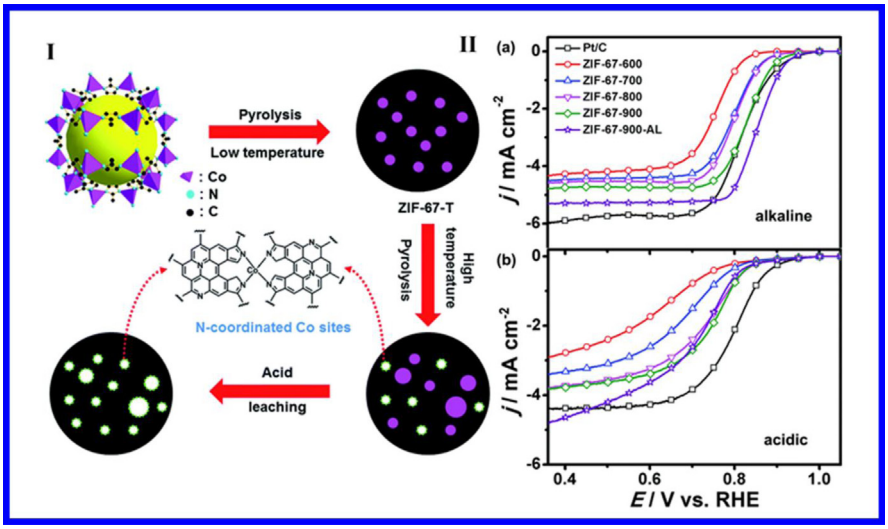

Fig. 8. (I) Schematic illustration of the synthesis process for ZIF-67-T catalysts. (II) LSV of ZIF-67-T and the acid-leached sample ZIF-67-900-AL in O_2-saturated 0.1 M KOH (a) and 0.5 M H_2SO_4 (b) [57].

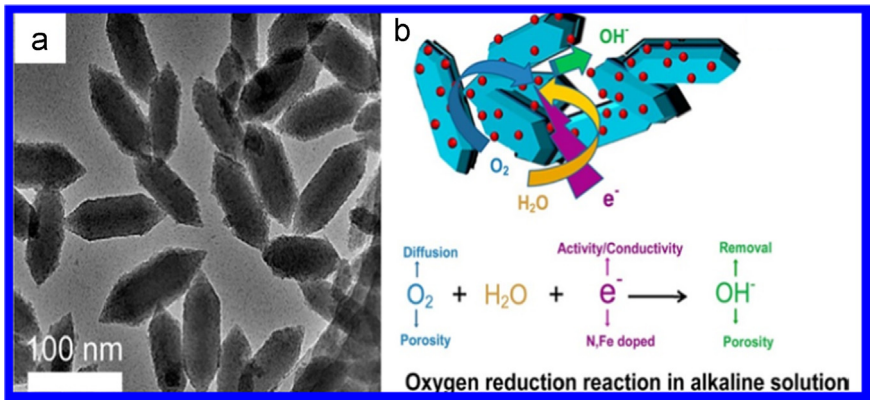

Fig. 9. (a) TEM images of nanoscale MIL-88B NH_3. (b) Principle of high performance electrocatalysts for oxygen reduction reaction in alkaline solution [59].

Table 1
Summary of the MOF-derived non-noble metal catalysts with high ORR activity reported in literatures.

Catalyst	Electrolyte	ORR onset potential	Limiting current density (mA cm^{-2})	Ref.
Cu-MOFs	0.1 M phosphate buffer	−0.15 V (vs. Ag/AgCl)	–	[46]
8 wt% GO-Cu-MOFs	0.5 M H_2SO_4	0.29 V (vs. RHE)	−5.32	[47]
(r-GO-50 wt%-FeP)$_n$ MOFs	0.1 M KOH	−0.23 V (vs. Ag/AgCl)	−6.2	[48]
ZIF-8 derived NGPC	0.1 M KOH	−0.02 V (vs. Ag/AgCl)	−4.3	[49]
ZIF-7/glucose-derived carbon	0.1 M KOH	0.86 V (vs. RHE)	−4.6	[51]
N,S-MOF-5-C	0.1 M KOH	−0.005 V (vs. Ag/AgCl)	–	[52]
ZIF-8 derived carbon@CNTs	0.1 M KOH	1.03 V (vs.RHE)	~−6.0	[55]
ZIF-8 derived carbon@graphene	0.1 M KOH	0.92 V (vs. RHE)	−5.2	[56]
Co-N-C-900	0.1 M KOH	0.93 V (vs. RHE)	~−5.2	[57]
Fe/FeN/C	0.1 M KOH	1.03 V (vs. RHE)	–	[59]
Fe/Fe_3C/C@GR/CNTs	0.1 M KOH	0.04 V (vs. Ag/AgCl)	–	[62]
Co@Co_3O_4@C-CM	0.1 M KOH	0.93 V (vs. RHE)	~−4.6	[63]
N/Co@C-GO	0.1 M KOH	0.93 V (vs. RHE)	~−7.0	[64]
Pt/C	0.5 M H_2SO_4	0.9 V (vs. RHE)	−6.17	[59]

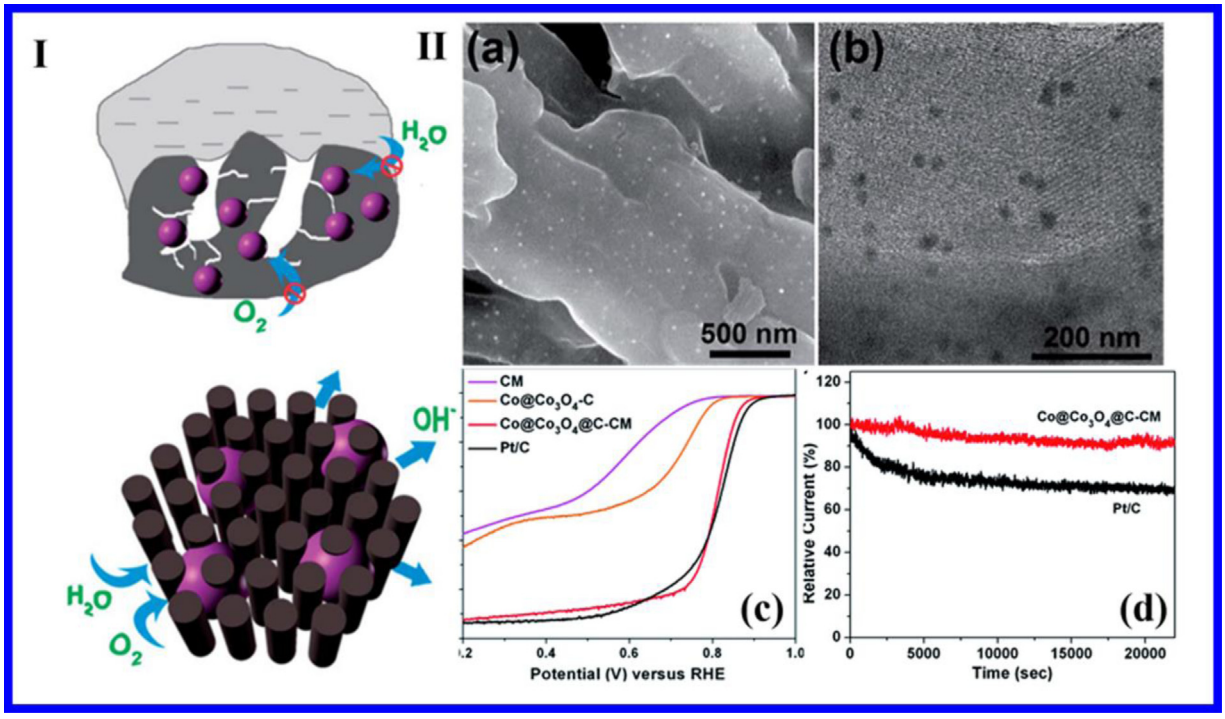

Fig. 10. (I) Schematic illustration of the synthesis of Co@Co_3O_4@C–CM and principle of electrocatalysis. (II) (a and b) SEM and TEM images of Co@Co_3O_4@C–CM. (c) ORR polarization curves of CM, Co@Co_3O_4@C, Co@Co_3O_4@C–CM, and Pt/C (scan rate: 10 mV s^{-1}; rotation rate: 1600 rpm). (d) Chronoamperometric responses of Co@Co_3O_4@C–CM and Pt/C at 0.75 V for 20,000 s [63].

best ORR activity of all the non-precious metal catalysts reported so far. (Table 1 gives the summary of the non-noble metal catalysts with high ORR activity reported in literatures.) The excellent ORR performance highlighted that the porous nanocarbon with rich Fe/FeN active sites are beneficial for both mass transport and catalytic conversion during an ORR process. Additionally, Afsahi employed Fe-containing MOFs as the sole precursor for preparing a cathode electrocatalyst. After pyrolysis, acid leaching and heat treatment under NH_3 at different temperatures, iron–nitrogen containing carbon active sites (Fe/N/C) were formed. Their work revealed that using only a Fe-containing MOFs does not lead to an optimized electrocatalyst, which means Fe instead of being used as the major constituent of the parent MOFs was applied only as a minor component are promising as electrocatalyst precursors [60].

To develop enough effective space for the diffusion of gas (O_2 or H_2) and electrolyte into the catalyst, rapid mass transport properties have become a key factor in pursuing more efficient ORR catalysts [58,61]. Though traditional MOFs have the inherent advantage of creating porous catalysts with high surface areas, the porous structures of the derived catalysts are usually destroyed after the carbonization process, only resulting in disordered and non-interconnected pore structures that are not beneficial for mass transport. Therefore, the rational design and fabrication of MOF-derived hybrids as efficient catalysts with ideal three-dimensional interconnected highly ordered pores, which guarantee the freely diffusion of O_2 and H_2O, will be more significant but very challenging. In 2015, Lan's group first reported on the successful synthesis of a novel N-doped Fe/Fe_3C@graphitic layer/carbon nanotube hybrid using MOFs [MIL-101 (Fe)] as solid precursors by a one-step and in-situ approach [62]. Taking advantage of the merits of synergistic effect of the unique architectures, large content of active sites (Fe/N/C species) and super excellent electron-conductive graphitic layers/carbon nanotubes, the obtained hybrids demonstrated excellent activities towards ORR and OER. In the meantime, Zou and co-workers reported a novel Co-MOFs induced strategy to prepare new Co@Co_3O_4@C core at bishell nanoparticles in-situ encapsulated into a highly ordered porous carbon matrix [63]. The central cobalt metal cores were transformed into Co@Co_3O_4 particles, which has proved to be ORR active (Fig. 10). The organic ligands from MOFs were transformed into porous graphitic carbon, which could in situ wrap the Co@Co_3O_4 nanoparticles resulting in not only enhancing the electron transfer between Co@Co_3O_4 nanoparticles and porous carbon matrix but also making the active particles hard to detach from the matrix support. Most importantly, the carbon matrix provides a three-dimensional interconnected pore structure, which produces much better transport pathways for oxygen and the electrolyte than the catalyst prepared from pure MOFs crystals. Furthermore, a novel hybrid with graphene oxide-supported Co-MOFs particles (Fig. 11) has been developed by Hou and co-workers [64]. Co-MOFs particles distributed on the surface of graphene sheets act as a spacer and protective layer to prevent the severe agglomeration of graphene nanosheets during high temperature treatment. In addition, Co-MOFs were converted to functional carbon materials with high specific surface area, nanoporous structure, and nitrogen-doping carbon framework. As a result, this kind of N/Co-doped porous carbon@GO composite with remarkable features of the porous carbon structure, N/Co-doping effect, introduction of graphene support leading to triple electrocatalytic activities for ORR, HER, and OER. Additionally, the good interaction between N/Co-doped carbon and graphene support make the catalyst composite with superior durability and excellent methanol tolerance.

2.5. Summary and perspective

Overall, it can be concluded that MOFs, with low cost and excellent properties, can act as electrode catalysts or catalyst precursors by adjusting their structures to obtain the optimized materials for fuel cells. As non-Pt fuel cell catalysts, Cu-based MOFs, Fe-based MOFs, as well as MOFs–graphene composites exhibit good catalytic activity, high chemical stability, and methanol tolerance. Using MOFs as precursors for preparation of electrocatalyst, metal/metal oxide/nitrogen/carbon hybrids with effective catalytic activity can be simply achieved. Therefore, by carefully selecting metal clusters and multi-functional linkers, the desired MOFs product can be designed with rich transition metal–nitrogen–carbon sites and which would be beneficial for fabricating good electrochemical catalysts.

MOFs-based materials have shown to be a highly promising candidate for catalysis in PEMFCs. However, to meet the requirements for PEMFCs commercialization, further research is required. In particular, further understanding of the nature of the active sites and precisely control active sites density is essential, as they play a critical role in MOFs design for PEMFCs and are the key to further improving activity and addressing stability problems. Once the active sites of MOFs are understood, desired structures can be designed precisely to improve the activity and stability of catalysts.

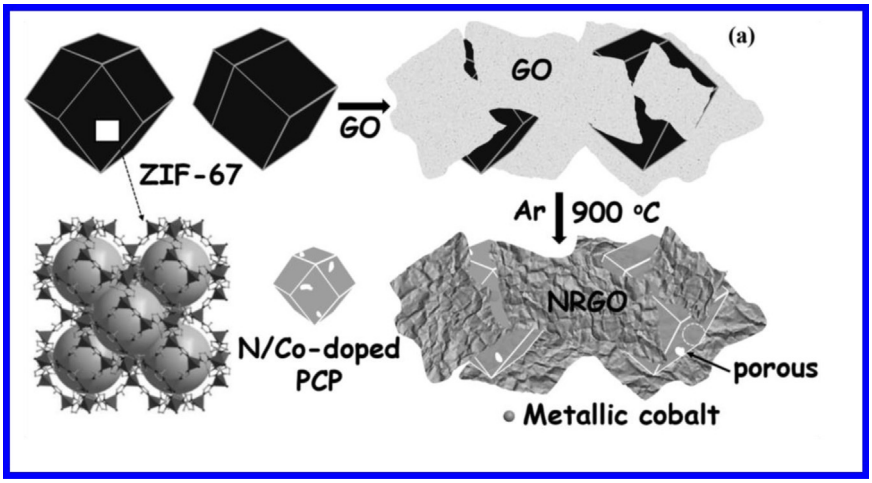

Fig. 11. Schematic illustration of the synthesis process of N/Co-doped porous carbon@GO composites [64].

3. MOFs for lithium-ion battery applications

3.1. MOFs as cathode materials for LIBs

The amount of lithium ions that can be reversibly inserted and re-inserted into a cathode material for LIBs is one of the limiting factors affecting its energy density, together with its working voltage [65]. Tarascon's group firstly developed a MIL-53 ($Fe^{III}(OH)_{0.8}F_{0.2}O_2CC_6H_4CO_2 \cdot H_2O$) MOF as a cathode material for LIBs [66]. This MOF exhibited an initial reversible capacity of 80 mAh g^{-1} and maintained 70 mAh g^{-1} after 50 cycles. The relatively low capacities can be attributed to the limited maximum lithium insertion amount, which is $x=0.6$ for $Li_xFe^{III}(OH)_{0.8}F_{0.2}O_2CC_6H_4CO_2 \cdot H_2O$ with a gravimetric capacity of 75 mAh g^{-1}. Subsequently, X-ray absorption fine structure (XAFS) analysis of the Fe K-edge during lithium insertion and extraction reveals changes in the local atomic environment of this MOFs [67]. These results demonstrate that the short distance of Fe–O is conserved upon reduction of Fe(III) and the Fe–Fe distances along the inorganic chain are maintained during distortion of the long-range structure [67]. Doublet's group investigated the mechanism of lithium insertion in MIL-53 in detail, based on density functional theory (DFT) calculation [68,69]. Furthermore, electroactive sorbent has been investigated in order to increase the electrochemical capacity of MIL-53-Fe by Tarascon's group [70]. The results show that the extra capacity associated with this guest rapidly fades upon cycling. Another Fe-based MOFs (MIL-68(Fe), $Fe(OH)(BDC)\cdot(solv)_x$) was also tested for its electrochemical properties and shows relatively low capacities [71]. In a recent work, MIL-101(Fe) has been also applied as a cathode material for LIBs [72]. It has been found that the redox chemistry of Fe^{2+}/Fe^{3+} is not completely reversible, which led to rapid decay of the capacity. In summary, Fe-based MOFs are the most popularly studied MOFs as cathode materials for LIBs. However, the performance of these MOFs is not yet satisfactory due to the low lithium-ion insertion amount and the unstable structure change of the MOFs during redox reactions.

In another research, Vittal et al. synthesized a new lithium containing MOF ($Li_2(VO)_2(HPO_4)_2(C_2O_4)$) as a cathode material [73]. The MOF exhibited a quite high electrochemical plateau at 3.9 V and delivered a reversible capacity of 80 mAh g^{-1} after 25 cycles. Meanwhile, this MOF exhibited high rate performance with a capacity of 47 mAh g^{-1} at 500 mA g^{-1}. In their study, the presence of extractable lithium ions in the inter-layer space, together with the feasibility of the $V^{4+/5+}$ redox couple, make this compound suitable for cathode applications in LIBs [73].

3.2. MOFs as anode materials for LIBs

3.2.1. MOFs as anodes

In 2006, Chen's group first reported using MOF-177 (Zn_4O (1,3,5-benzenetribenzoate)$_2$) as an anode material for LIBs, in which the different morphologies of the MOF can be controlled through a solvothermal route [74]. The electrochemical results show that the first discharge and charge capacities of the cubic MOF-177 are ~400 mAh g^{-1} and 105 mAh g^{-1}, respectively. The involved reactions in the MOF-177 electrode can be expressed as

$$Zn_4O(BTB)_2 \cdot (DEF)m(H_2O)n + e + Li^+ \rightarrow Zn + Li_2O$$

$$DEF + H_2O + e^- + Li^+ \rightarrow Li_2(DEF) + LiOH$$

$$Zn + Li^+ + e^- \leftrightarrow LiZn$$

Another group studied three diamondoid MOFs, $Zn_3(HCOO)_6$, $Co_3(HCOO)_6$, and $Zn_{1.5}Co_{1.5}(HCOO)_6$, as anodes [75]. It was shown that the $Zn_3(HCOO)_6$ anode obtained a stable capacity of 560 mAh g^{-1} up to 60 cycles at 60 mA g^{-1}. Meanwhile, the other two MOFs, $Co_3(HCOO)_6$ and $Zn_{1.5}Co_{1.5}(HCOO)_6$, also delivered large capacities of 410 mAh g^{-1} and 510 mAh g^{-1}, respectively, which demonstrate great improvements compared with that of MOF-177. Similar reaction mechanisms are proposed for $Zn_3(HCOO)_6$:

$$Zn_3(HCOO)_6 + 6Li^+ + 6e^- \leftrightarrow 3Zn + 6HCOOLi$$

$$3Zn + 3Li^+ + 3e^- \leftrightarrow 3LiZn$$

However, there is only one conversion process for $Co_3(HCOO)_6$ without alloy formation:

$$Co_3(HC) \leftrightarrow 3Co + 6HCOOLi$$

Some other kinds of MOFs, including $Co_2(OH)_2BDC$ [76], $Li_2(OBA)$ (H_2OBA=4,4′-oxybisbenzoic acid) [77], and Prussian blue analogs ($M_3^{II}[Co^{III}(CN)_6]_2 \cdot nH_2O$ (M=Co, Mn)) [78], have also been studied as anode materials for LIBs. These studies show a quite high reversible capacity and rate performance of these MOFs anodes. Based on the above studies, the organic ligands play an important role in the conversion process, as well as the center metallic alloying-type process.

More recently, the electrochemical properties of bifunctionalized MOFs (BMOFs, $Zn(IM)_{1.5}(abIM)_{0.5}$, IM=Imidazole) have also been studied [79]. It was proposed that Li-ions are indeed stored within the BMOFs pores as the frameworks remain intact during the discharge and charge processes. The host–guest interactions between Li and amine groups/N atoms can also be attributed to this storage behaviour [79]. Thus, for the porous-storage mechanism, the performance can be further enhanced by increasing the amount of active N-rich functional groups and the surface area per pore volume [79].

Table 2
Electrochemical performances of different kind of MOFs in the application of LIBs.

Samples	Electrode	Current density	Initial reversible capacity (mAh g^{-1})	Cycle numbers	Capacities (mAh g^{-1})	Ref.
MIL-53 (Fe)	Cathode		80	50	70	[66]
MIL-64 (Fe)	Cathode	C/10	30	–	–	[71]
$Li_2(VO)_2(HPO_4)_2(C_2O_4)$	Cathode	0.1 C	75	25	83	[73]
MOF-177(Zn)	Anode	50 mA g^{-1}	105	–	–	[74]
$Zn_3(HCOO)_6$	Anode	60 mA g^{-1}	693	60	560	[75]
$Co_3(HCOO)_6$	Anode	60 mA g^{-1}	–	60	410	[75]
$Zn_{1.5}Co_{1.5}(HCOO)_6$	Anode	60 mA g^{-1}	–	60	510	[75]
$Co_2(OH)_2BDC$	Anode	50 mA g^{-1}	1005	100	650	[76]
$Co_3[Co(CN)_6]_2$	Anode	20 mA g^{-1}	294.2	5	304	[78]
$Mn_3[Co(CN)_6]_2$	Anode	50 mA g^{-1}	354.9	100	35.3	[78]
$Zn(IM)_{1.5}(abIM)_{0.5}$	Anode	100 mA g^{-1}	–	100	190	[79]

In brief, MOFs are attracting increasing attention both as cathodes and anodes for LIBs, as well as the fact that the metal ions and organic ligands can be involved in the electrochemical processes, undergoing the different mechanisms. Table 2 indicates the electrochemical performances of different kinds of MOFs directly used as cathode or anode materials for LIBs. However,

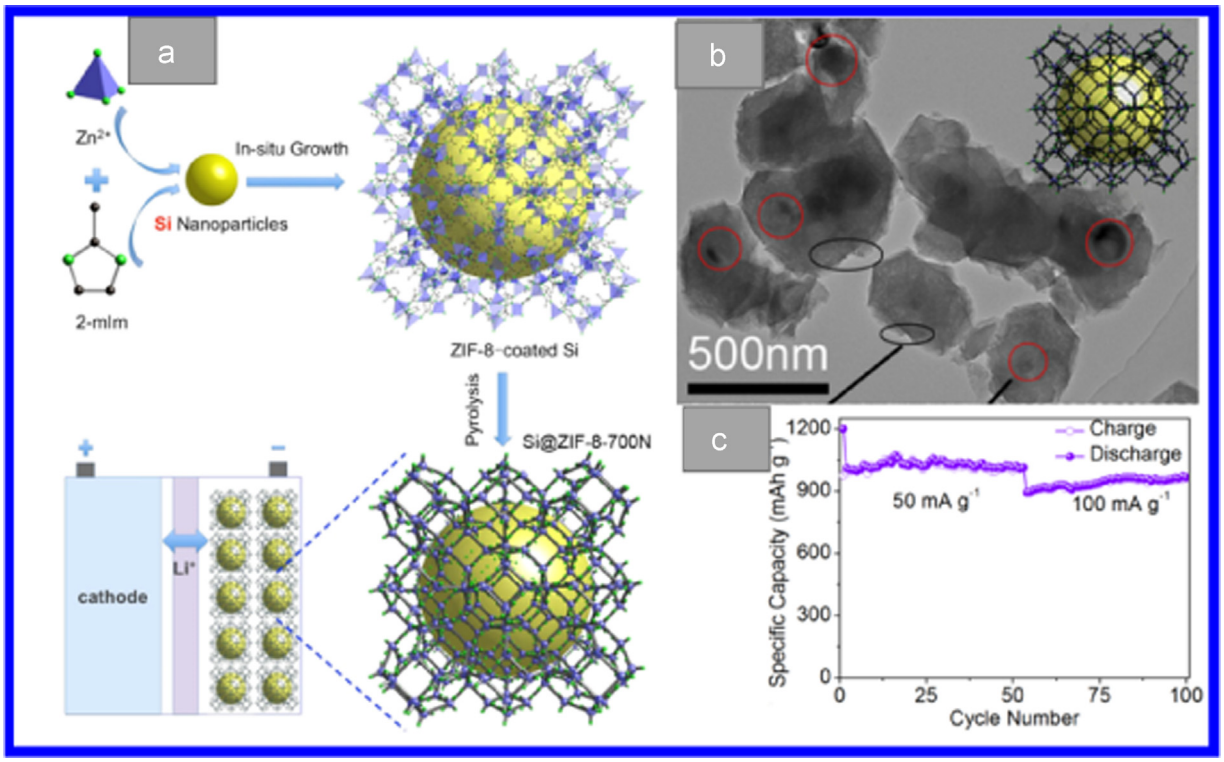

Fig. 12. (a) Schematic representation of the preparation of Si@ZIF-8-700N for anode material in LIBs. (b) TEM image of Si@ZIF-8-700N. After pyrolysis, ZIF-8 converts to amorphous carbon with well-dispersed zinc ions. (c) Cycling performance of Si@ZIF-8-700N [81].

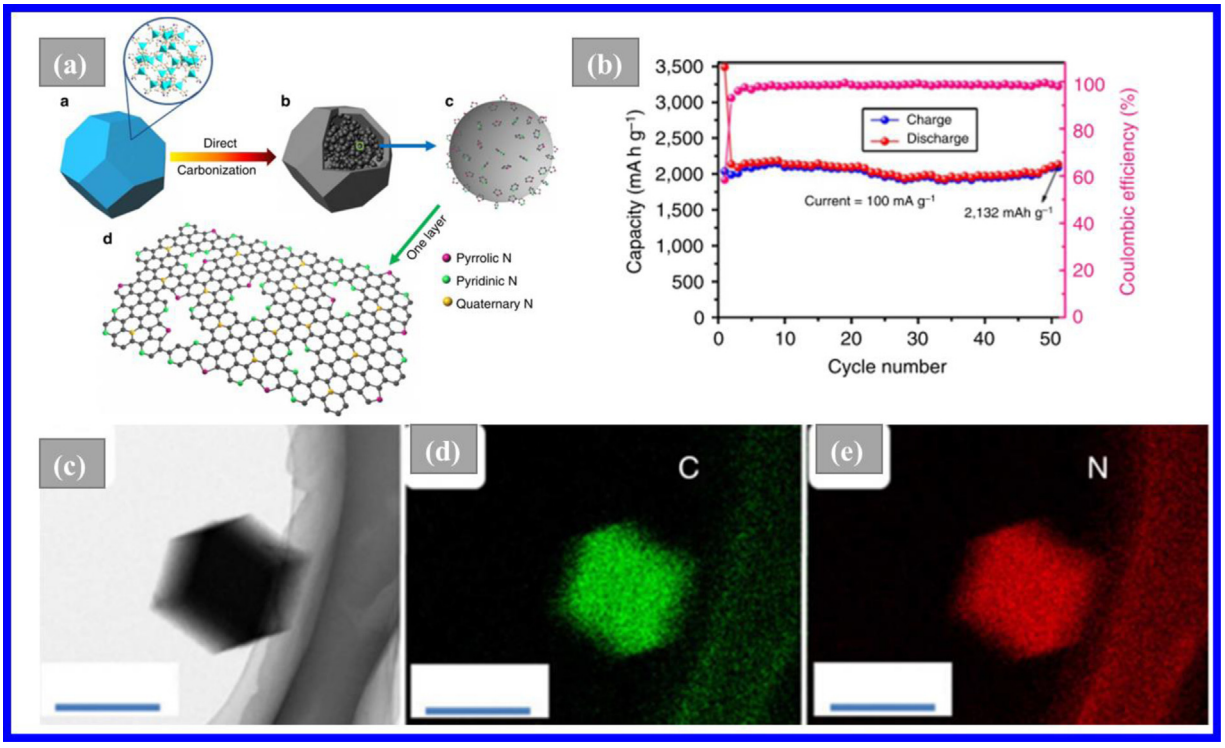

Fig. 13. (a) Schematic illustration of the synthesis procedure of N-doped graphene analogous particles and the model of N-doping. (b) Cycling performance at a current density of 100 mA g^{-1}. (c–e) Scanning TEM image of the MOF-derived mesoporous N-C-800 polyhedron and energy dispersive X-ray spectrometry elemental maps of C and N [83].

there are still some serious issues for the reported MOFs as anodes, such as their low conductivities and decomposed or collapsed structures during cycling. And the studies on the reaction mechanisms of different MOFs in LIBs are still ongoing. In this case, further efforts are expected to develop and improve MOFs as anode materials for LIBs.

3.2.2. MOF-derived materials as anodes for LIBs

For the alloying-type anode materials of LIBs, one of the most serious issues is their large volume change during electrochemical cycling. An alternative strategy is to use porous materials as anodes or introduce coating layers as a buffering matrix, including porous carbon, carbon nanotubes, graphene, or polymer. MOFs are regarded as a new kind of ideal matrix for anodes. Wei's group used ZIF-8 as the coating layer on the surface of Zn_2SnO_4 (ZTO) nanoparticles to form a core/shell structure of ZTO/ZIF-8 nanocomposites [80]. The electrochemical results indicate that the thin ZIF-8 coating layer can effectively enhance the performance of the composites by accommodating the drastic volume expansion of the electrode. Furthermore, MOFs are also excellent precursors for the synthesis of mesoporous carbons after pyrolysis. In a recent work [81], researchers designed a one-pot method to assemble ZIF-8 on the surface of Si nanoparticles followed by further carbonization at 700 °C, in which the schematic representation is shown in Fig. 12(a). The morphology of the as-prepared sample can be observed in the SEM image in Fig. 12(b), in which the Si nanoparticles are fully covered by carbonized ZIF-8, with stable capacity retention of 1020 mAh g^{-1} after 50 cycles (Fig. 12(c)). The significant improvement can be attributed to N-doped carbon derived from ZIF-8 as well as the uniform distribution of Zn(II) that facilitates lithium ion transport and buffers volume expansion. In this case, MOFs and MOF-derived carbon can be potential coatings and buffering matrices for alloying and conversion anodes, with the advantages of in situ growth and large performance improvements.

To date, the commercial anodes for LIBs mainly focus on carbon-based materials due to their stable properties. Several novel carbon materials have been developed, including mesoporous carbon, graphene, and carbon nanotubes with higher reversible capacities than commercialized graphite [82]. As discussed above, MOFs are considered great reactive precursors for the synthesis of nanoporous carbon materials. Meanwhile, in the organic components, heteroatoms such as sulfur, phosphorus, boron, and nitrogen generally exist, which makes direct pyrolysis of MOFs an effective way for producing heteroatom-doped carbon materials. Chen et al. reported nitrogen-doped graphene particle

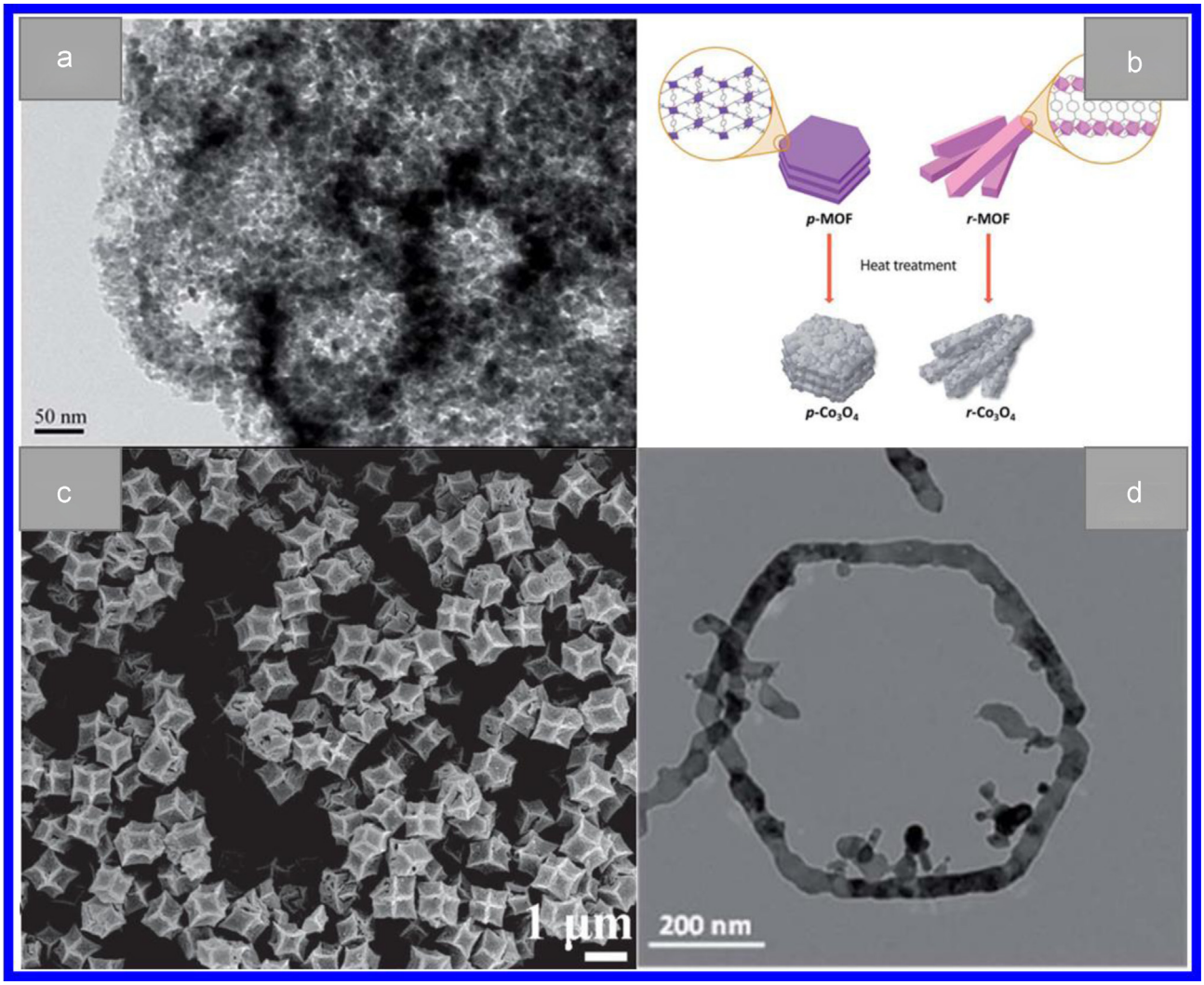

Fig. 14. (a) High-magnification TEM image of MOF-71@300N materials [86]. (b) Scheme of pseudomorphic conversion of Co-MOFs [89]. (c) FE-SEM image of Co_3O_4 dodecahedra derived from ZIF-67 [90]. (d) TEM image of Co_3O_4 prepared via the calcination of hydrolyzed product using Co–NTCDA microspindles as the precursor [91].

analogs with a high nitrogen content of 17.72 wt%, which are directly derived from pyrolysis of a nitrogen-containing ZIF-8 [83]. The schematic illustration of the synthesis procedure is shown in Fig. 13(a). The TEM image and EDX elemental mappings indicate the high distribution of nitrogen in the particles (Fig. 13(c–e)). Interestingly, this novel carbon anode achieved a capacity of 2132 mAh g^{-1} after 50 cycles (Fig. 13(b)), which can be attributed to the nitrogen-doped hexagonal lattice and edges. Thus, it can be useful to control the type and concentration of heteroatoms by choosing different organic components or additional surfactants with alternative heteroatoms. Furthermore, the ZIF-8-derived microporous carbons have also been tested as anode materials for sodium-ion batteries, and exhibits considerably higher capacity and better reversibility than mesoporous carbon (CMK-3) [84]. It is believed that the small pore size of ZIF-C can significantly reduce decomposition of the electrolyte.

Besides carbon materials, MOFs have also been widely studied as precursors for metal oxides, carbon/metal composites, and mixed transition metal oxides. In 2000, Xu's group first reported a MOF-precursor route for preparation of Co_3O_4 nanoparticles with an average diameter of around 250 nm, which is converted from cobalt-MOFs ($Co_3(NDC)_3(DMF)_4$) via a pyrolysis method in air [85]. The agglomerated Co_3O_4 nanoparticles favor improved cycling and rate capability as LIB anodes. In another study, mesoporous nanostructured Co_3O_4 was prepared by the direct pyrolysis of MOF-71 ([Co(bdc)(DMF)]), in which the as-prepared mesoporous Co_3O_4 shows high specific surface area, reasonable pore volume, and small crystallite size (as seen in Fig. 14(a)) [86]. The capacity of the porous Co_3O_4 was 913 mAh g^{-1} after 60 cycles at a current rate of 200 mA g^{-1}. Other studies have mainly focused on building different dimensions or micro/nano structures of Co_3O_4 based on MOFs [87,88]. Moon et al. synthesized two kinds of Co_3O_4: plate-

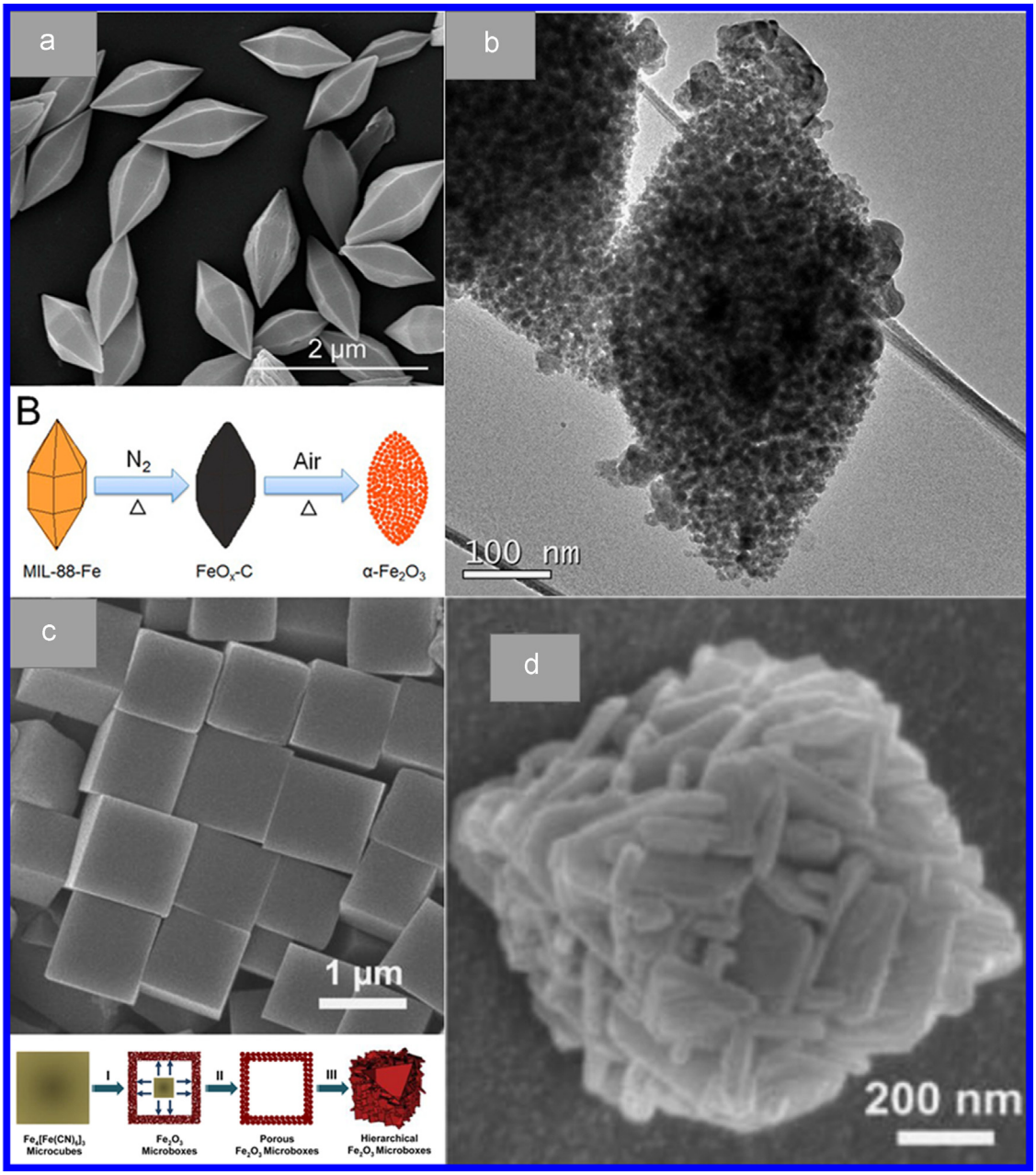

Fig. 15. (a) SEM image of as-prepared MIL-88-Fe and illustration of the fabrication of spindle-like porous α-Fe_2O_3. (b) TEM image of the final spindle-like α-Fe_2O_3 [93]. (c) SEM image of PB microcubes and schematic illustration of the formation of hollow Fe_2O_3 microboxes. (d) SEM image of a hierarchically-structured shell consisting of Fe_2O_3 nanoplatelets [94].

like (p-Co_3O_4) and rod-like (r-Co_3O_4), which transformed from two types of corresponding Co-MOFs: plate-shaped ($[Co_3(BDC)_3(DMF)_4]_n$, p-MOF) and rod-shaped ($[Co(BDC)(DMSO)]_n$, r-MOF), respectively [89]. The scheme of pseudomorphic conversion of Co-MOFs is shown in Fig. 14(b). Both as-prepared Co_3O_4 are composed of primary nanoparticles of 10 nm, with different sized nanopores. The electrochemical results show that the different microstructures affect the cyclability and rate capability of these MOF-derived Co_3O_4, and the rod-like one exhibited the best performance. Another study reports that uniform Co_3O_4 hollow dodecahedra have been synthesized by direct thermal treatment of as-synthesized ZIF-67 ($[Co(mim)_2]_n$, mim: 2-methylimidazolate) [90]. The uniform size and rhombic dodecahedral morphology can be seen from the SEM image in Fig. 14(c). Benefiting from these unique structural features, the hollow dodecahedra exhibit high lithium storage capacities and excellent cycling performance.

For the controllable design of structures and morphologies of MOF-derived cobalt oxides, the release rate of Co^{2+} has significant influence. This can be adjusted via the basic strength of organic amines along with the spatial hindrance of organic linkers that determine the thickness of hydrolyzed products, as reported by Li's group [91]. Two kinds of Co-MOFs, i.e. Co–NTCDA (NTCDA: 1,4,5,8-naphthalenete-tracarboxylic dianhydride) and Co–PTCDA (PTCDA: perylene-3,4,9,10-tetracarboxylic dianhydride), were first prepared by a hydrothermal method and had different morphologies as microspindles and microflowers, respectively. After treatment in tetramethylammonium hydroxide, both of the hydrolyzed products of Co–NTCDA microspindles and Co–NTCDA microflowers transformed into a nanoring structure with particle sizes of 760 nm. The SEM image of the final Co_3O_4 nanoring after further calcination is shown in Fig. 14(d). The as-prepared Co_3O_4 hexagonal nanorings retain a high discharge reversible capacity of 1370 mAh g^{-1} after 30 cycles. This special morphology can provide shortened transfer paths for Li^+ and higher surface areas for enhanced performance.

Other MOF-derived metal oxides, including iron oxide [92], copper oxide, and titanium dioxide, have also been studied as anode materials for LIBs, due to their lower toxicity compared with cobalt oxides. Cho et al. first used Fe-MOFs as a template to prepare iron oxide as an anode material for LIBs [93]. MIL-88 ($Fe_3O(H_2O)_2Cl(BDC)_3 \cdot nH_2O$) was chosen as the precursor for synthesis of α-Fe_2O_3, in which the MIL-88-Fe had the spindle-like structure. Illustration of the fabrication process is shown in Fig. 15(a). In this process, MIL-88-Fe was first annealed at 500 °C in N_2 gas to obtain an FeO_x–C composite, then heated at 380 °C in air to get the final product of α-Fe_2O_3. After calcination, the α-Fe_2O_3 still had the spindle-like morphology with mesoporous character, as shown in Fig. 15(b). This kind of anode exhibited a high charge capacity of 911 mAh g^{-1} after 50 cycles. Prussian blue (PB) is another popular Fe-MOF consisting of a mixed-valence iron (III) hexacyano ferrate (II) compound of composition $Fe_4[Fe(CN)_6]_3$, with a cubic crystal structure (Fig. 15(c)) [94,95]. The subsequent thermal process to transfer PB microcubes into Fe_2O_3 microboxes can be generally divided into three stages, as shown in Fig. 15(c) [94]. At a relatively low annealing temperature of 350 °C, the produced Fe_2O_3 microboxes retained well the size and cubic shape of the PB microcubes. The porous shells of Fe_2O_3 microboxes were obtained by raising the temperature to 550 °C. When increasing the annealing temperature to 650 °C, the as-prepared sample was comprised of a hierarchically-structured shell consisting of Fe_2O_3 nanoplatelets (Fig. 15(d)), which exhibited a high specific capacity of ~950 mAh g^{-1} and excellent cycling performance.

Copper oxide derived from Cu-based MOFs has also been reported as an anode material for LIBs by two groups [96,97]. The $[Cu_3(btc)_2]$ (btc: benzene-1,3,5-tricarboxylate) MOF was selected as the template for both studies. The as-prepared CuO is comprised of hollow octahedra with high surface area and mesoporous structure, as well as excellent electrochemical performance. TiO_2 has been discovered as another promising metal oxide electrode for LIBs. A novel porous anatase TiO_2 has been prepared through the calcination of MIL-125 as the precursor, which has high reversible capacity and good rate capability [98]. Thus, in this case, MOFs can be used as a good precursor for converting metals into metal oxides. Generally, metal oxides derived from MOFs can maintain the initial morphology of the MOF as well as create unique structures of hollow inner networks. Meanwhile, the metal oxides can obtain the same porous structure as the MOFs during removal of the organic ligand, resulting in relatively high surface areas. All these benefits lead to their excellent electrochemical performance due to an increased Li^+ diffusion coefficient and buffered volume expansion.

Coating a carbon layer on alloying or conversion mechanism anodes is an effective way to accommodate the serious volume change and increase their conductivity. MOFs provide a novel in situ approach for the synthesis of carbon-coated metal anodes. When annealing MOFs under the protection of an inert atmosphere, like N_2 and Ar, the organic ligands will decompose into carbon layers [99,100]. In this way, the MOF-derived metal/metal oxide particles are surrounded by a carbon matrix, which acts as a buffering and conductive coating to further improve the performance of these anodes. Porous carbon-coated ZnO quantum dots derived from MOF-5 have been prepared by a one-step controlled pyrolysis method. The materials exhibit high specific charge capacities of ~1200 mAh g^{-1} and stable cycling performance [101]. Cobalt-doped ZnO nanoparticles coated with carbon have also been synthesized by heat treatment of Co-doped MOF-5 [102], which demonstrated enhanced performance compared to undoped ZnO particles derived from MOF-5. Recently, it was reported that the direct carbonization of a synthesized Sn-based MOF, $[K_2Sn_2(1,4\text{-bdc})_3](H_2O)$, resulted in the stabilization of tin nanoparticles in a porous carbon matrix [103]. When tested as an anode material for LIBs, the as-prepared Sn@C exhibited a specific capacity of nearly 600 mAh g^{-1} after 100 cycles. Various metal@-carbon matrices can be obtained using this in situ process via the annealing of MOFs. Qian et al. first prepared Ni nanoparticles in carbon matrices by calcination of MOF-74(Ni) and converted it into NiS through an in situ reaction [104]. This approach provides a simple method for fabricating metal sulfide/carbon composites with a porous structure and high surface area, the applications of not only LIBs but also other energy storage devices such as SIBs and supercapacitors.

Mixed transition-metal oxides (MTMOs), including ferrites, cobaltates, and nickelates, refer to single-phase ternary metal oxides with two different metal cations, rather than mixtures of two binary metal oxides [105]. MTMOs have the significant "self-matrices" mechanism during the electrochemical process compared with traditional metal oxides, which leads to improved properties compared to individual metal oxides. For the fabrication of MTMOs, MOFs have attracted more and more attention due to their controllable design of structure, high surface area, and porosity. In the early stages, Li's group developed $ZnMn_2$-ptcda (ptcda = perylene-3,4,9,10-tetracarboxylic dianhydride) as a precursor to be transformed into spinel-structured $ZnMn_2O_4$ nanoplates [106]. In their work, this "escape-by-crafty-scheme" strategy has been extended to the synthesis of $CoMn_2O_4$ and $NiMn_2O_4$, which exhibits the typical *I4₁/amd* tetragonal spinel structure and cubic spinel structure in the *Fd3m* space group, respectively [106]. Hollow porous $CoFe_2O_4$ nanocubes have also been prepared by annealing $Co[Fe(CN)_6]_{0.667}$ precursor under air at different temperatures [107]. A representative illustration of the formation of these compounds is shown in Fig. 16(a). It was found that the annealing temperature had a significant influence on the

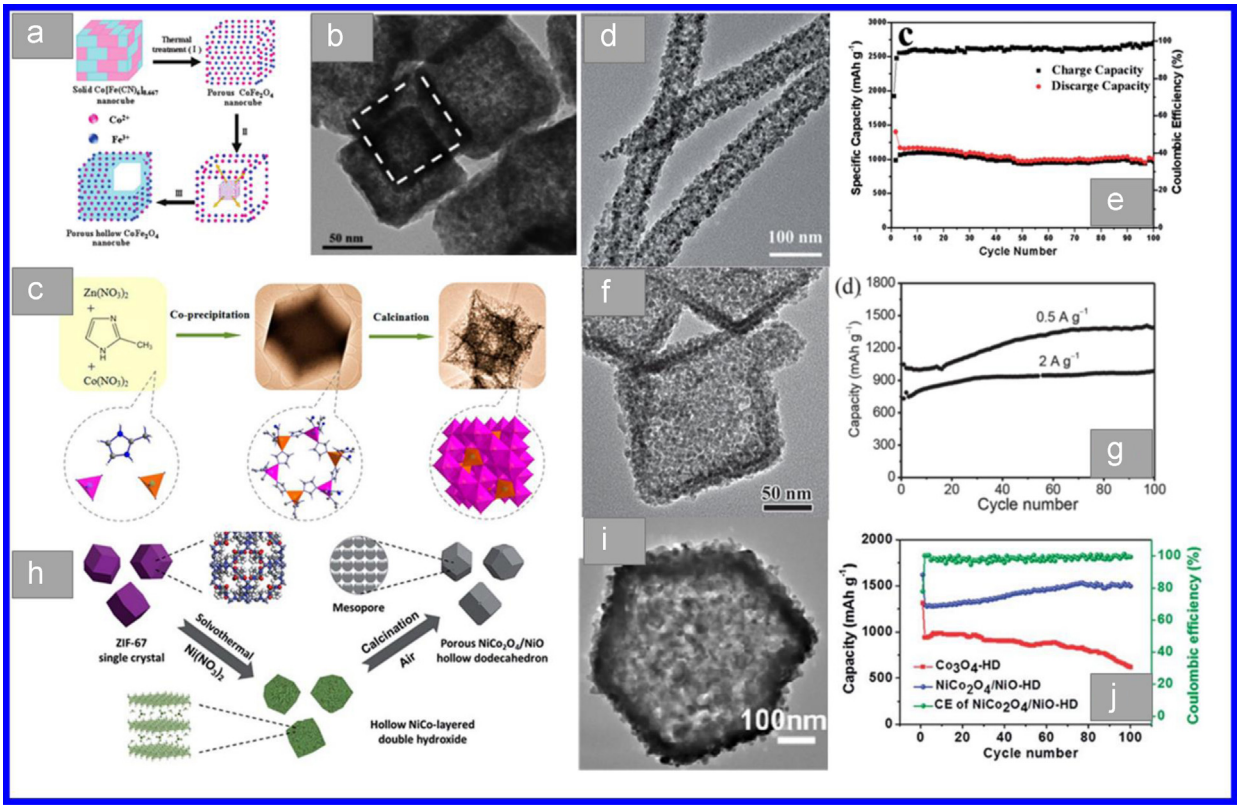

Fig. 16. (a) Representative illustration of the formation of hollow $CoFe_2O_4$ nanocubes from MOFs [107]. (b) TEM image of as-synthesized hollow $CoFe_2O_4$ nanocubes [108]. (c) Schematic illustration of the preparation of bimetallic ZIFs and their conversion to spinel $Zn_xCo_{3-x}O_4$ hollow polyhedra [109]. (d) TEM image of $NiFe_2O_4/Fe_2O_3$ nanotubes. (e) Capacity and Coulombic efficiency of the $NiFe_2O_4/Fe_2O_3$ nanotubes at a current rate of 100 mA g^{-1} [111]. (f) TEM image and (g) cycling performance of as-formed porous hollow octahedra made of $ZnO/ZnFe_2O_4/C$ nanoparticles [112]. (h) Schematic illustration of the preparation process, (i) TEM image, and (j) cycling performance at a current density of 0.2 A g^{-1} of porous $NiCo_2O_4/NiO$ hollow dodecahedra [113].

morphologies of the MOF-derived $CoFe_2O_4$. The porous and hollow structures were not formed at 200 °C and the interior nanocube structures were destroyed at the higher temperature of 400 °C. The unique hollow $CoFe_2O_4$ nanocubes (shown in Fig. 16(b)) were obtained at 350 °C, and exhibited the best cycling performance of 1115 mAh g^{-1} after 200 cycles. Similar progress has been reported for the synthesis of $Mn_{1.8}Fe_{1.2}O_4$ nanocubes, which is based on another kind of PB analog, $Mn_3[Fe(CN)_6]_2 \cdot nH_2O$ [108]. The as-prepared $Mn_{1.8}Fe_{1.2}O_4$ inherits the porous structure and relatively high specific surface area (124 m^2 g^{-1}) of the precursor MOF. As a result, the capacity of the porous $Mn_{1.8}Fe_{1.2}O_4$ was retained at 827 mAh g^{-1} after 60 cycles. Interestingly, R.B. Wuet al. prepared porous $Zn_xCo_{3-x}O_4$ hollow polyhedra derived from "Zn-Co-ZIF-n" (shown in Fig. 16(c)), in which different molar ratios of Zn:Co were used to obtain uniform polyhedral crystals [109]. In this process, all of the Zn:Co molar ratios within the co-precipitated ZIFs were higher than that of the corresponding reactants, which can be attributed to the stronger coordination ability of Zn^{2+} than Co^{2+} [109]. Wang et al. chose another MIL-88 as a template to design two types of MTMOs anodes: core–shell $NiFe_2O_4@TiO_2$ nanorods [110] and hierarchical $NiFe_2O_4/Fe_2O_3$ nanotubes [111]. As an example, hierarchical $NiFe_2O_4/Fe_2O_3$ nanotubes had diameters of 78 nm and lengths of around 1 mm (Fig. 16(d)) and exhibited reversible specific capacities of 936.9 mAh g^{-1} for up to 100 cycles (Fig. 16(e)).

Similar to the fabrication of carbon/metals or carbon/metal oxides, novel ultrafine ZnO and $ZnFe_2O_4$ nanocrystals embedded in a porous carbon framework have been derived from Fe^{III}-MOF-5. This composite was composed of hollow octahedral nanoarchitectures and exhibited capacity retention of 1390 mAh g^{-1} over 100 cycles (Fig. 16(f, g)) [112]. In the above report, researchers first synthesized MOFs containing two types of metal elements and, after pyrolysis, the MTMOs or their composites were obtained. In a recent study, another new approach has been developed [113]. ZIF-67 was used as both precursor and sacrificial template and then a hydrothermal method and subsequent calcination were carried out to obtain the final $NiCo_2O_4/NiO$ composites. A schematic illustration of the preparation process is shown in Fig. 16(h). The as-prepared sample shows a porous, hollow dodecahedron structure (Fig. 16(i)) and displays a very highly reversible capacity of 1497 mAh g^{-1} over 100 cycles (Fig. 16(j)). This strategy represents a general method for synthesis of hierarchically interconnected and porous nanostructures of MTMOs and their composites.

MOFs have also been introduced for the synthesis of hierarchical-structured anode materials for LIBs, including metal oxide/graphene composites [114], mixed metal oxide composites [115–117], and metal oxide/CNT composites [118], derived from both MOFs and organic-coated MOF composites [119]. Lou et al. demonstrated an approach for fabricating hierarchical hollow microboxes via manipulation of the template-engaged reactions between a PB template and different alkaline substances [120]. Series multi-compositional microboxes, such as Fe_2O_3/SnO_2, Fe_2O_3/SiO_2, Fe_2O_3/GeO_2, Fe_2O_3/Al_2O_3, and Fe_2O_3/B_2O_3, have been reported in their work. A typical schematic illustration of the formation of different hierarchical metal oxide microboxes, starting from PB microbox templates, is shown in Fig. 17(a). Route A illustrates the formation of different structural hollow boxes with varying complexity, from single shell to multi-shells. Route B involves the preparation of multi-compositional hollow boxes consisting of other elements with uniform oxides/hydroxides of iron boxes [121]. As an example, when tested as an anode material for LIBs, the Fe_2O_3/SnO_2 composite microboxes exhibit remarkable electrochemical

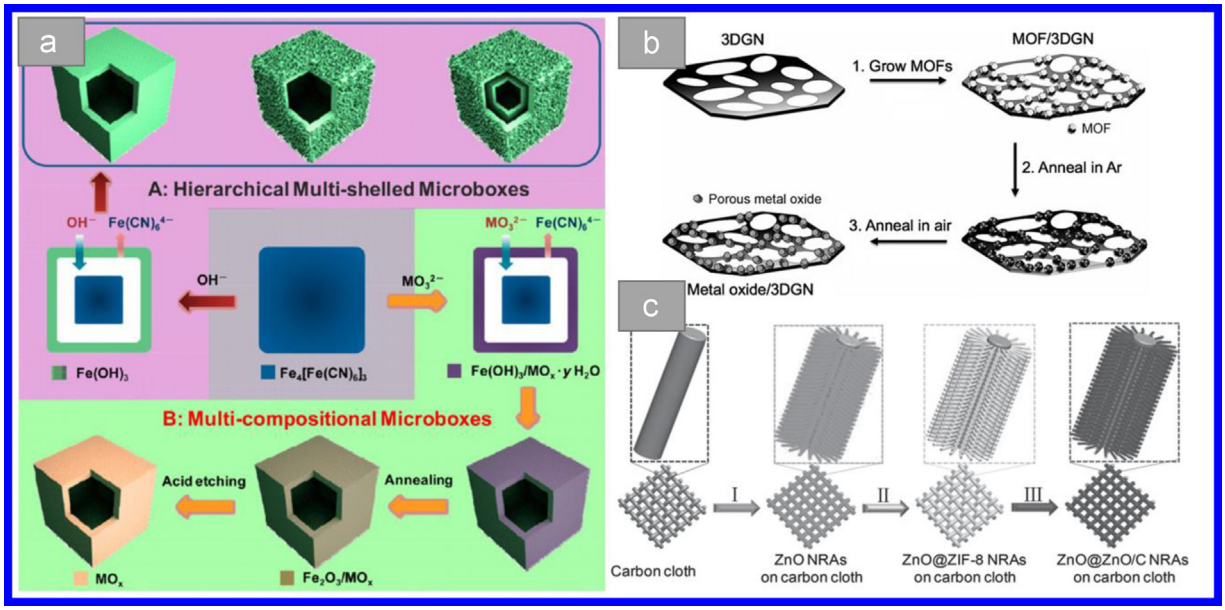

Fig. 17. (a) Schematic illustration of the formation of hierarchical multi-shelled (route A) and multi-compositional (route B) metal oxide microboxes, starting with metal–organic framework templates [120]. (b) Schematic illustration of the process used for the synthesis of metal oxide/3DGN composites [122]. (c) Schematic illustration of the synthesis procedures for ZnO@ZnO QDs/C core–shell NRAs on carbon cloth [126].

Table 3
Comparison of nanostructure materials derived from MOFs in the application of LIBs.

Materials	Original MOFs	Current density	Cycle numbers	Capacities (mAh g^{-1})	Ref.
N doped graphene particle analogs	ZIF-8	100 mA g^{-1}	50	2132	[83]
Co_3O_4 nanoparticles	$Co_3(NDC)_3(DMF)_4$	100 mA g^{-1}	100	730	[85]
mesoporous Co_3O_4	Co(bdc)(DMF)	200 mA g^{-1}	60	913	[86]
Co-CP-A	Co(bdc)(DMF)	100 mA g^{-1}	50	536	[87]
Co-CP-B	Co(bdc)(DMF)	100 mA g^{-1}	50	651	[87]
Co-CP-C	Co(bdc)(DMF)	100 mA g^{-1}	50	391	[87]
Co_3O_4 nanoplates	Co(HO-BDC)(bbb)	500 mA g^{-1}	500	852	[88]
p-Co_3O_4	$Co_3(BDC)_3(DMF)_4$	0.1 C	100	300	[89]
r-Co_3O_4	Co(BDC)(DMSO)	0.1 C	100	800	[89]
Co_3O_4 hollow dodecahedra	ZIF-67	100 mA g^{-1}	100	780	[90]
Co_3O_4 hexagonal nanorings	Co-NTCDA	100 mA g^{-1}	30	1370	[91]
α-Fe_2O_3	$Fe_3O(H_2O)_2Cl(BDC)_3 \cdot nH_2O$	0.2 C	50	911	[93]
Fe_2O_3 microboxes	Prussian blue	200 mA g^{-1}	30	950	[94]
Porous Fe_2O_3 nanocubes	Prussian blue	200 mA g^{-1}	50	800	[95]
CuO hollow octahedra	$Cu_3(btc)_2$	100 mA g^{-1}	100	470	[96]
ZnO@C	MOF-5	75 mA g^{-1}	50	1200	[101]
Co doped ZnO@C	Co doped MOF-5	100 mA g^{-1}	50	725	[102]
$CoFe_2O_4$ nanocubes	$Co[Fe(CN)_6]_{0.667}$	1 C	200	1115	[107]
$Mn_{1.8}Fe_{1.2}O_4$ nanocubes	$Mn_3[Fe(CN)_6]_2 \cdot nH_2O$	60 mA g^{-1}	200	827	[108]
$ZnxCo_{3x}O_4$ hollow polyhedra	Zn-Co-ZIF	100 mA g^{-1}	50	990	[109]
$NiFe_2O_4$@TiO_2 nanorod	Fe_2Ni-MIL-88	100 mA g^{-1}	100	1034	[110]
ZnO@ZnO Quantum Dots/C	ZIF-8	500 mA g^{-1}	100	699	[125]
ZnO/$ZnFe_2O_4$/C	ZIF-8	500 mA g^{-1}	100	1390	[112]

performance due to the uniquely designed structure. Three-dimensional metal-oxide-coated graphene composites were also developed, in which MOFs served as the precursors and were first grown on 3D graphene networks (3DGN) [122]. As shown in Fig. 17 (b), the desired metal oxide/3DGN composites were then obtained by a two-step annealing process. Two types of well-known MOFs, ZIF-8 and MIL-88-Fe, were used for the preparation of ZnO/3DGN and Fe_2O_3/3DGN composites, respectively. For the application in LIBs, the as-prepared Fe_2O_3/3DGN composites demonstrated larger performance enhancement and improved rate properties compared to the pure Fe_2O_3 electrode.

Conversion chemistry is a versatile approach for the conversion of one compositional nanostructure into another [123]. Through this process, metal oxides, instead of soluble salts, can act as alternative metal precursors for the synthesis of MOFs when introducing organic ligands on the surface of the metal compound [124,125]. Al_2O_3, ZnO, and Cu_2O have been reported as conversion materials for the preparation of MOFs. Very recently, a hierarchical structure of ZnO@ZnO quantum dot/C core–shell nanorod array on a carbon cloth derived from MOFs was fabricated by a conversion method. Fig. 17(c) shows the process [126]. Initially, aligned and ordered ZnO nanorods (NRs) were grown on a flexible carbon cloth substrate by a facile and scalable low-temperature solution deposition route. Then, ZnO@ZIF-8 NRs were controllably synthesized by using ZnO NRs as sacrificial templates in the presence of 2-methylimidazolate. Finally, the shell layer ZIF-8 was transformed into an amorphous carbon framework and ZnO QDs during the pyrolysis process, resulting in a stronger adhesive force between

carbon and ZnO nanocrystals. Owing to the shortened Li^+ diffusion distance, superior electron collection efficiency, sufficient conductivity, and good structural stability of the nanorod arrays, the free standing ZnO@ZnO QDs/C NRAs exhibited remarkable rate capability and cycling performance [126].

3.3. Summary and perspective

In this section, we summarized the recent developments of and understanding on MOFs and their derivatives for the application of electrode materials for LIBs. Table 3 gives a brief summary and comparison of nanostructure materials derived from MOFs in the application of LIBs. This includes directly using MOFs as the cathode or anode, as well as using them as precursors for synthesizing anode materials. For LIB cathodes, the electrochemical properties of MOFs are still not satisfactory in currently reported studies. However, the existing results show that the design of MOFs used as cathode materials can be further developed. For anode materials, there are three types of mechanisms for lithium ion storage: (1) the reversible reaction between MOFs and lithium or the initial irreversible process followed by an alloying reaction; (2) the porous-storage mechanism, in which the electrochemical performance is related to the pore size, surface area, and heteroatom doping; and (3) MOFs, as a kind of porous material, acting as the buffering matrix for huge volume change anode materials to relieve stress during the alloying or conversion processes. However, the low electronic conductivity of MOFs is still a big issue for this strategy. On the other hand, MOFs can be a good choice as reactive precursors for the synthesis of nanoporous carbon materials, which provide improved coating layers and buffering matrices with high stability and conductivity. Additionally, the mesoporous carbon derived from MOFs can be directly used as an excellent anode material. The main section of this part focuses on the design and synthesis of different metal oxides and their composites derived from MOFs. Using this strategy, desirable structures and morphologies with high porosity and surface area can be obtained. It has also been shown that MOFs can be selected as suitable templates for the preparation of hollow and hierarchical structures. Particularly, the shape, particle size, crystal structure, and purity can be tuned by varying the experimental conditions and annealing processes. In this case, as-prepared metal oxides and their composites inherit the high surface area and porosity of the precursor MOFs, which further leads to the great electrochemical performance. MOFs and MOF-derived materials show great potential as LIB cathodes, anodes, and especially as precursors for the design of nanostructured carbon and metal oxide materials. However, it should be pointed out that there are still two problems for MOFs and MOFs derived materials in the applications of LIBs. One of the issues should be the high surface area of MOFs and MOF-derived materials will lead to the large irreversible capacities during the first discharge process. The other problem is the quite low volumetric energy and power densities due to the low density of MOFs. Thus, in the practical applications of MOFs and MOF-derived materials in LIBs, these two shortages can still be the big challenge for both avoiding the negative effect of high surface area and low energy density.

4. MOFs for next-generation battery applications

4.1. MOFs in the application of lithium–sulfur batteries

4.1.1. MOFs directly applied to Li–S batteries

Li–S batteries have been investigated for decades due to their ultrahigh energy density [127]. However, the state-of-the-art Li–S battery systems still face many issues which hinder their commercial

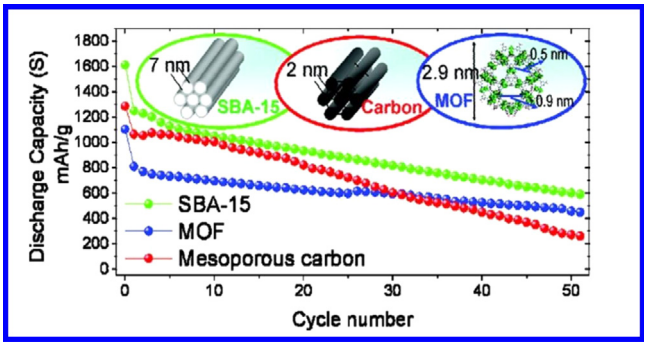

Fig. 18. Cycle performance comparison of commercial carbon materials and MIL-100 as hosts for sulfur cathodes [133].

applications [128], especially in the case of sulfur cathode materials. The inherent low conductivity of sulfur and the shuttle effect from dissolved polysulfides result in poor cycle life of Li–S batteries [129,130]. In order to overcome these issues, the most prevailing strategies involve using host materials to improve the conductivity and encapsulate sulfur within the host matrix [131,132].

MOFs have high porosity and high surface area, and are therefore very suitable to be used as hosts for sulfur cathodes. Tarascon et al., for the first time, used the MOF MIL-100 (Cr) as a host material for sulfur encapsulation [133]. MIL-100 is comprised of chromium metallic ions linked with 1,3,5-benzentricarboxylate ligands and composed of mesoporous cages (~25–29 Å) with small windows (5 and 9 Å) and large pore volumes (~1 $cm^3\ g^{-1}$). The small diffusion window is very suitable for trapping soluble polysulfides and the large pore volume sustains over 50 wt% sulfur load. Electrochemical performance of MOF–S composites shows an increase in capacity retention of Li–S cathodes compared with commercial C–S composites (Fig. 18). Investigations using TEM and XPS reveal that MIL-100 provides a weak binding between polysulfides and the oxygenated framework, which impedes the diffusion of polysulfides from the host matrix.

More recently, some research efforts have focused on the interaction between MOF hosts and sulfur or polysulfides. Qian et al. reported a copper-based MOF, HKUST-1, incorporated with sulfur as a cathode material for Li–S batteries [134]. It was demonstrated from XPS measurements that sulfur and open metal sites had reversible interactions during discharge–charge processes, and this interaction effectively reduced the release of dissolved polysulfides into the electrolyte. However, it should be noted that due to the limited conductivity of MOFs, the capacity of these sulfur composites were limited to 500 mAh g^{-1} after 50 cycles. Xiao et al. further revealed the interaction between MOF hosts and sulfur species and proposed the “Lewis acid–base” interaction concept for MOF–S composites, as shown in Fig. 19 [135]. As proposed in the literature, coordinated metallic ions from MOFs can be considered as soft Lewis acids and dissolved polysulfide anions as soft Lewis bases. The Lewis acid center enables a link with polysulfides and therefore suppress the polysulfide shuttle effect. Based on this mechanism, the authors also proposed an order to form stable complexes with metallic centers: Mn (II) < Fe (II) < Co (II) < Ni (II) < Cu (II), shedding a light on the choice of MOFs for hosts in Li–S batteries. Cyclic performance of Ni- and Co-based MOFs as hosts for sulfur cathodes further confirmed the mechanism, in which Ni–MOFs performed better in terms of cycling stability with a capacity retention of around 500 mAh g^{-1} after 200 cycles. However, it still should be noted that this paper did not mention the particle size or other physical characterizations of the as-prepared Co–MOFs and Ni–MOFs, which is very important for Li-ion diffusion pathways and polysulfide preservation in Li–S batteries. Li's group published several papers on the understanding of

the particle size and aperture window of MOFs for Li–S batteries [136,137]. As proposed, MOF particle size affects the utilization of sulfur and the initial discharge capacity in Li–S batteries. The aperture window of MOFs, on the other hand, affects the conversion of polysulfides, which means a well-designed aperture window should facilitate Li-ion diffusion and refine polysulfides in the host. These papers investigated different sizes of ZIF-8 and also MOFs with different aperture sizes in Li–S batteries and concluded that ZIF-8 with a particle size of 100–200 nm and an aperture window of 3.4 Å shows the best Li–S battery performance. The authors mentioned that the low conductivity of the MOFs and sulfur led to low utilization of the MOF-S composites compared to the prevailing C/S composites. This research investigated nanostructures not only for MOF hosts, but also gave a general guide on the design of novel hosts for Li–S batteries.

4.1.2. *MOF-derived carbon materials for Li–S batteries*

Since Xu's group first developed MOF-derived carbons from MOF-5 (Fig. 20a), these novel materials have been receiving extensive attention in many different energy storage fields [138,139]. Most MOF-derived carbon obtains ultrahigh surface area, small aperture windows, fitted pore size ranges, and unique morphologies from MOFs. More importantly, the conductivity of MOF-derived carbons is much higher than that of MOFs, which makes them very suitable as substrates in energy storage systems. For Li–S batteries, carbon materials are the most common hosts in sulfur cathodes. The high surface area and high conductivity of MOF-derived carbons make them very suitable for use in Li–S batteries [140–142]. Cheetham et al. published the first paper on the use of different MOF-derived carbon in Li-S batteries and made a comparison of the electrochemical performance of these MOF-derived carbon hosts, as shown in Fig. 20(b-c) [143]. Zinc-based MOF-derived carbons, from MOF-5 to ZIF-8, were synthesized with different approaches and investigated as carbon hosts. Based on the different surface areas and pore volumes, they concluded that a higher ratio of mesopores (2–50 nm) facilitates a higher initial discharge capacity for Li–S batteries, since Li ions can much more easily diffuse into the carbon matrix. Further, the elevated micropore volume of MOF-derived carbon demonstrated stable cycle life for Li–S batteries, due to the small aperture window readily able to block polysulfides from dissolution. This paper gave a general introduction of different MOF-derived carbons in the application of Li–S batteries.

Recent papers have focused on further understanding the relation between pore structure and the sulfur cathode electrochemical reaction. Two recent studies from Lou's group and Yin's group investigated short-chain sulfur molecules embedded in

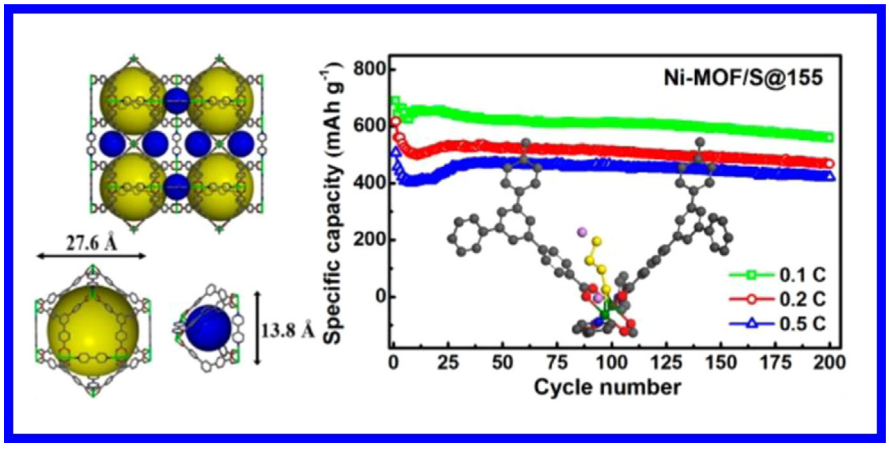

Fig. 19. Lewis acid–base interactions between polysulfides and metal organic framework in Li–S batteries [135].

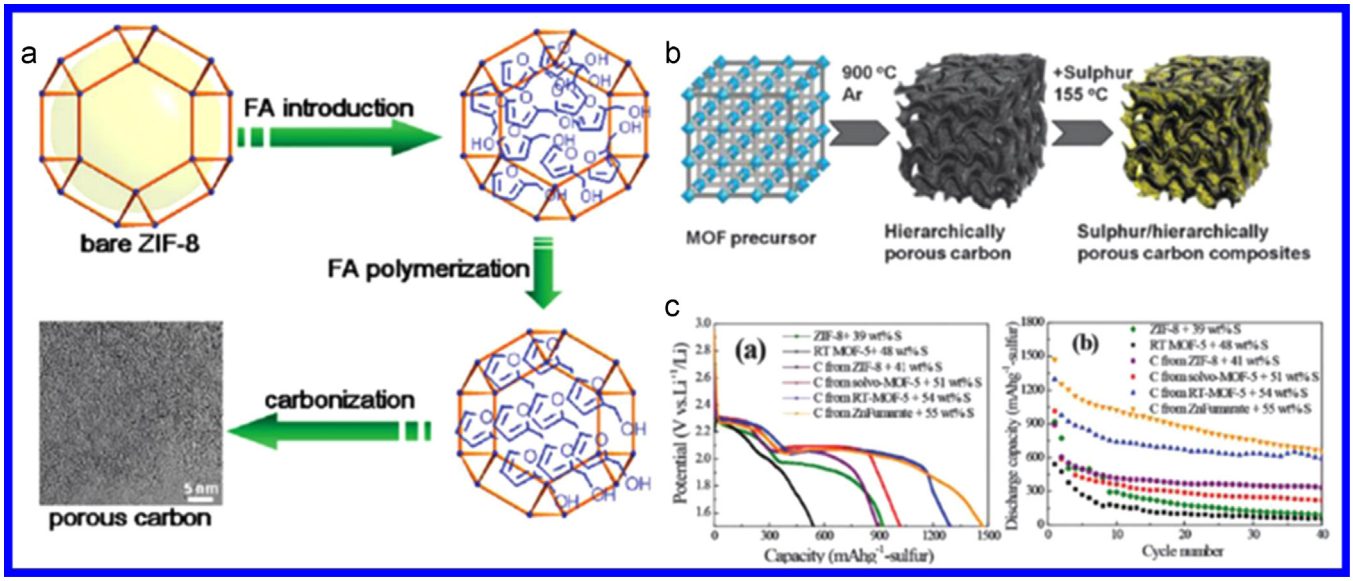

Fig. 20. (a) Preparation of MOF-derived carbon [160] and (b, c) different MOF-derived carbons applied to Li–S batteries [143].

enriched micropores from MOF-derived carbons, illustrating in Fig. 21 [144,145]. Both showed very interesting Li–S electrochemical reactions with the use of carbonate-based electrolytes, and performed Li–S electrochemical tests different from typical reactions in the commonly-used ether-based electrolyte. These two papers mentioned that the microporous structure of MOF-derived carbons facilitates short-chain sulfur molecule formation in C/S composites, and such "small sulfur molecules" in micropores exhibit very stable cycle lives. It should still be noted that the reported sulfur loading in MOF-derived carbons micropores is very low, only around 30 wt%. Although the microporous structure is favorable for trapping polysulfides, it raises the resistance of the batteries because of slower Li-ion diffusion, which leads to lower utilization of sulfur compared to mesoporous carbon hosts. Therefore, further studies on using MOF-derived carbons for C/S electrodes should focus on designing favorable porous structures

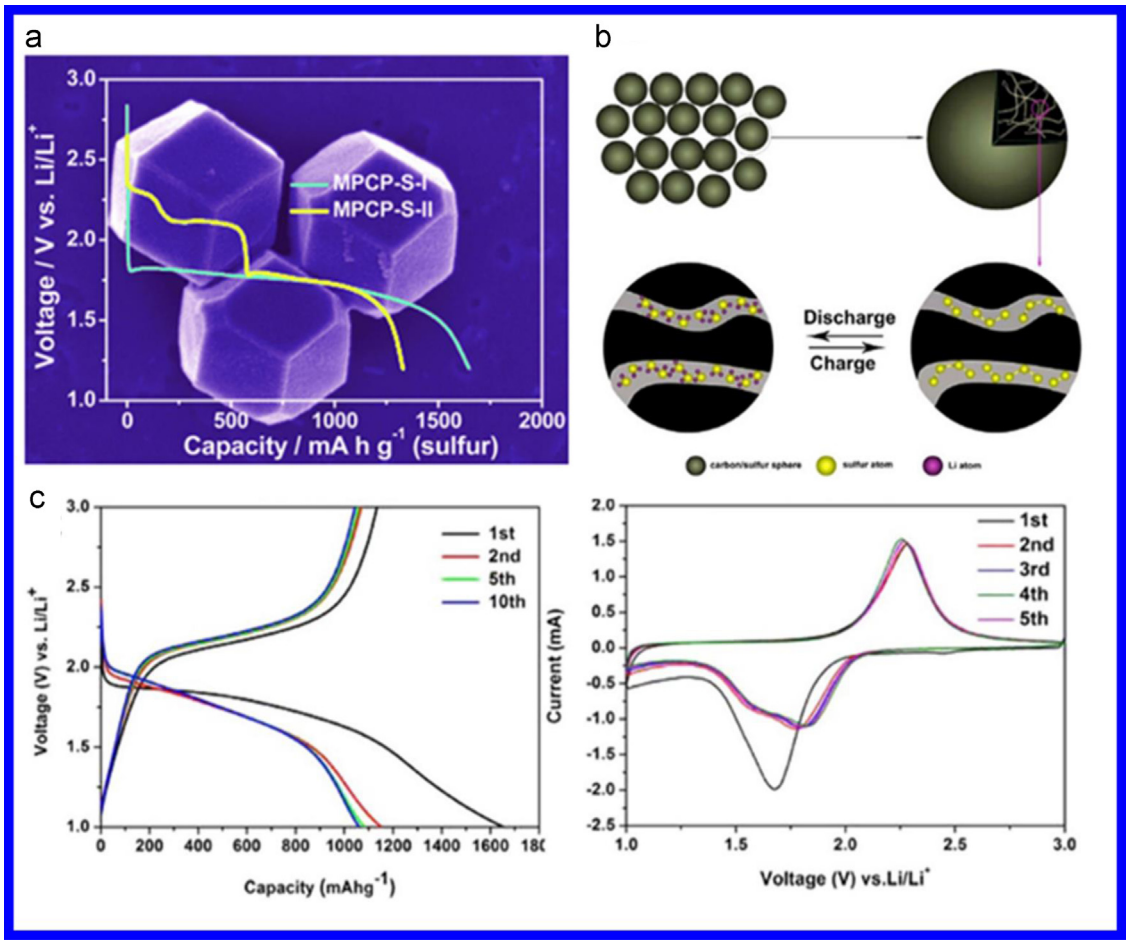

Fig. 21. Small sulfur in use for MOF–S cathodes. (a) Discharge curves and morphology of small sulfur in MOF-derived carbon [144] and (b, c) nitrogen-doped MOF-derived microporous carbon as small sulfur hosts for Li–S battery cathodes [145].

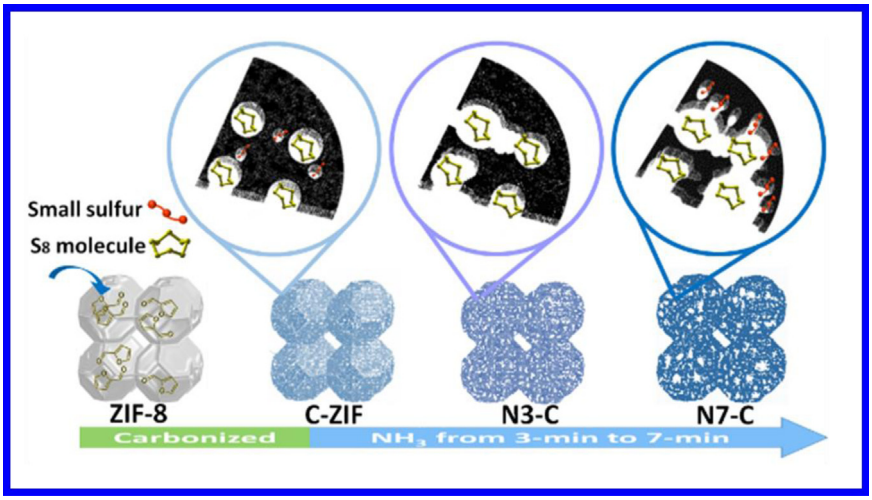

Fig. 22. In situ ammonia treatment of MOF-C applied for Li–S batteries [146].

from MOFs, instead of simply attempting to select various MOFs as precursors for nanocarbon before testing in a Li–S battery.

Following this thought, our group recently designed and reported a facile approach to fabricate porous carbon with controllable structure derived from MOFs [146]. The in situ ammonia (NH_3) etching treatment facilitates desirable pore distribution of MOF-derived carbon from an enriched microporous structure to a hierarchically mesoporous structure, demonstrating in Fig. 22. Our results show that NH_3-treated MOF-derived carbon as a sulfur host material for Li–S cathodes results in double the capacity retention compared to pristine MOF-derived carbon. Additionally, multi Li-S electrochemical mechanisms related to the different pore structures of carbon are also investigated in this paper. A multi-phase electrochemical reaction process of sulfur has been demonstrated, based on hybrid porous MOF–C. More importantly, the hybrid porous structure of MOF-derived carbon with ammonia treatment demonstrated about 800 mAh g^{-1} of discharge capacity over 100 cycles, which is over two times higher than pristine ZIF-8-derived carbon. This ammonia treatment approach demonstrates promising Li–S battery performance and expands the application of MOF-derived carbons in batteries.

4.1.3. Summary and perspectives

In summary of this part, MOFs and MOF-derived carbon are very novel and highly suitable host materials for Li–S batteries. The interaction between polysulfides and metal sites in the MOFs and MOF-derived carbons, along with their high surface areas and pore volumes, makes them greatly attractive candidates for host matrices in Li–S cathodes. MOF-derived carbons, as a new family of carbon materials, will be especially important as sulfur hosts in Li–S batteries due to their high conductivity, controllable pore structure, and their ability to trap polysulfides at their metallic sites and heteroatom dopant sites.

4.2. MOFs for Lithium–O_2 battery applications

Lithium–oxygen (Li–O_2) batteries regarding as the next-generation energy storage systems recently attract extensive research effort with remarkably high theoretical energy density. Theoretically, the energy density of Li–O_2 batteries reaches 3500 Wh kg^{-1}, which is 4–6 times higher than that of commercial LIBs. However, the rate capability, cycle life, and power performance of Li–O_2 batteries are still not satisfied for practical applications [147]. The polarization losses of cathode during discharge and charge process limits the electrical efficiency, which is one of the biggest challenges for Li–O_2 battery. To address this problem, an effective approach to improve the efficiency of Li–O_2 batteries is developing new catalyst, both for oxygen reduction reaction (ORR) during discharge and oxygen evolution reaction (OER) during charge. Several kind of catalysts, including nanocarbon materials, noble metal and transition metal oxide, have been studied in the recent decades. MOFs and MOFs derived materials containing different metal ions are considered as promising cathode catalyst for Li–O_2 batteries, in which micropores can mainly contribute to O_2 transportation and mesopores ideally suited for electrolyte diffusion and product deposition [148]. Wu et al. demonstrate three types of MOFs, including MOF-5, HKUST-1, and M–MOF-74 (M=Mg, Mn, Co) as the cathode materials for Li–O_2 batteries [148]. Among that, Mn–MOF-74 delivers a primary capacity of 9420 mAh g^{-1}, in which the population of O_2 molecules in the pores is enhanced by the accessible open metal sites in the uniform channels further assist the reaction efficiently. Another Ni–MOFs (Ni(4,4′-bipy)(H_3BTC)) with 3D micro–nano structure, open catalytic sites and large surface area are studied as potential cathode materials for Li–O_2 batteries possess an extremely high capacity of 9000 mAh g^{-1} and high round-trip efficiency of 80%. More interesting, after fabrication of plastic Li–O_2 cell with this kind of Ni–MOFs, a high energy density of 478 Wh kg^{-1} is

Table 4
MOFs and MOF-derived materials in the application of Supercapacitor.

Samples	MOFs	Surface area (m^2 g^{-1})	Electrolyte	Rate	Capacity (F g^{-1})	Ref.
MOFs directly used						
Co-MOF	Co-MOF	2900	1 M LiOH	0.6 A g^{-1}	206.76	[154]
Co-BDC	Co-BDC	9.09	–	10 mV s^{-1}	131.8	[155]
Co-NDC	Co-NDC	20.29	–	10 mV s^{-1}	147.3	[155]
Co-BPDC	Co-BPDC	138.35	–	10 mV s^{-1}	179.2	[155]
Ni-MOF-24	Ni-MOF-24	–	6 M KOH	0.5 A g^{-1}	1127	[156]
Zr-MOF$_1$	Zr-MOF$_1$	1047	6 M KOH	5 mV s^{-1}	1144	[157]
Zr-MOF$_2$	Zr-MOF$_2$	933	6 M KOH	5 mV s^{-1}	811	[157]
Zr-MOF$_3$	Zr-MOF$_3$	732	6 M KOH	5 mV s^{-1}	517	[157]
Zr-MOF$_4$	Zr-MOF$_4$	596	6 M KOH	5 mV s^{-1}	207	[157]
MOFs derived porous carbon						
NPC	MOF-5	2872	1.0 M H_2SO_4	1 mV s^{-1}	312	[160]
NPC$_{530}$	MOF-5	3040	1.0 M H_2SO_4	5 mV s^{-1}	12	[161]
NPC$_{650}$	MOF-5	1521	1.0 M H_2SO_4	5 mV s^{-1}	167	[161]
NPC$_{800}$	MOF-5	1141	1.0 M H_2SO_4	5 mV s^{-1}	107	[161]
NPC$_{900}$	MOF-5	1647	1.0 M H_2SO_4	5 mV s^{-1}	122	[161]
NPC$_{1000}$	MOF-5	2524	1.0 M H_2SO_4	5 mV s^{-1}	120	[161]
NPC	ZIF-8	1523	1.0 M H_2SO_4	5 mV s^{-1}	251	[162]
Z-600	ZIF-8	24	0.5 M H_2SO_4	50 mV s^{-1}	1	[166]
Z-700	ZIF-8	520	0.5 M H_2SO_4	50 mV s^{-1}	23	[166]
Z-800	ZIF-8	720	0.5 M H_2SO_4	50 mV s^{-1}	130	[166]
Z-900	ZIF-8	1075	0.5 M H_2SO_4	50 mV s^{-1}	128	[166]
Z-1000	ZIF-8	1110	0.5 M H_2SO_4	50 mV s^{-1}	112	[166]
MOF-derived metal oxides						
Porous Co_3O_4	Co- H_3ABTC-bpy	47.12	2 M KOH	0. 5 A g^{-1}	137.2	[179]
Porous hollow Co_3O_4	ZIF-67	128	3 M KOH	1.25 A g^{-1}	1100	[180]
CeO_2	Ce-BTC	77	3 M KOH	0.2 A g^{-1}	502	[181]
Cu–Cu_2O–CuO/C	MOF-199	–	6 M KOH	2 mV s^{-1}	750	[183]
Fe_3O_4/carbon	Fe-MIL-88B NH_2	37.7	1 M KOH	0.5 A g^{-1}	139	[184]
Ni–C	Ni-BDC	140	1 M KOH	1 A g^{-1}	886	[185]
Cr_2O_3 nanoribbons	MIL–101(Cr)	438	6 M KOH	2 mV s^{-1}	300	[186]

successfully achieved. This study demonstrates that pristine transition metal-MOFs can be very promising as alternative cathode materials for Li–O_2 batteries due to the unique feature of MOFs.

MOF-derived nanostructure materials can be also attractive in Li–O_2 batteries. Different kind of metal oxide nanocomposites including γ-Fe_2O_3/carbon nanocomposites [149], δ-MnO_2 nanoboxes [150], ZnO/$ZnFe_2O_4$/C nanocages [151] and porous cobalt–manganese oxide [152] derived from MOF precursors are tested as electrocatalysts in Li–O_2 batteries, which all deliver very high discharge capacities and satisfactory cycling stabilities. The reasons for the excellent catalytic properties of these materials can be ascribed as: (1) the high intrinsic electrocatalytic activity of transition metal oxide centers for ORR and OER [149]; (2) the hierarchical mesoporous structure of carbon can provide more active sites and faster electron transport; (3) the high surface areas also contribute to the mass/electron transportation in the multiphase discharge/charge reactions [151].

In a brief summary, different types of MOFs and MOFs derived metal oxide composites have been studied as electrocatalysts in Li-O_2 batteries battery, which indicate excellent performances due to their high surface area, hierarchical porosity and uniformly dispersed active sites. However, the overall studies on MOFs and MOFs derived materials for Li–O_2 battery are still in the very early state. It can be anticipated that increasing research efforts will be devoted to this field in the near future. Following efforts will be attempted to further improve the cycling performance as well as high capacity of the MOFs and MOF derived materials as air electrodes.

5. MOFs for supercapacitor applications

5.1. MOFs as electrodes for supercapacitors

Supercapacitors, as one of the promising energy storage devices, have attracted increasing attention due to the high power energy and long cycle life. One kind of supercapacitor is called electrical double-layer supercapacitors (EDLCs), which usually uses carbon materials with high surface area and porosity. However, the charges physically stored and energy densities of EDLCs are quite low. Pseudocapacitive with electrochemically active materials such as transition metal oxide and sulfides with increased energy density are more attractive in the recent years. In this case, MOFs and MOFs derived nanomaterials indicate great potential and advantages in the application of supercapacitors because of their high surface areas, controllable pores and nanostructures. In another approach, MOFs can be excellent template and precursors for preparation of

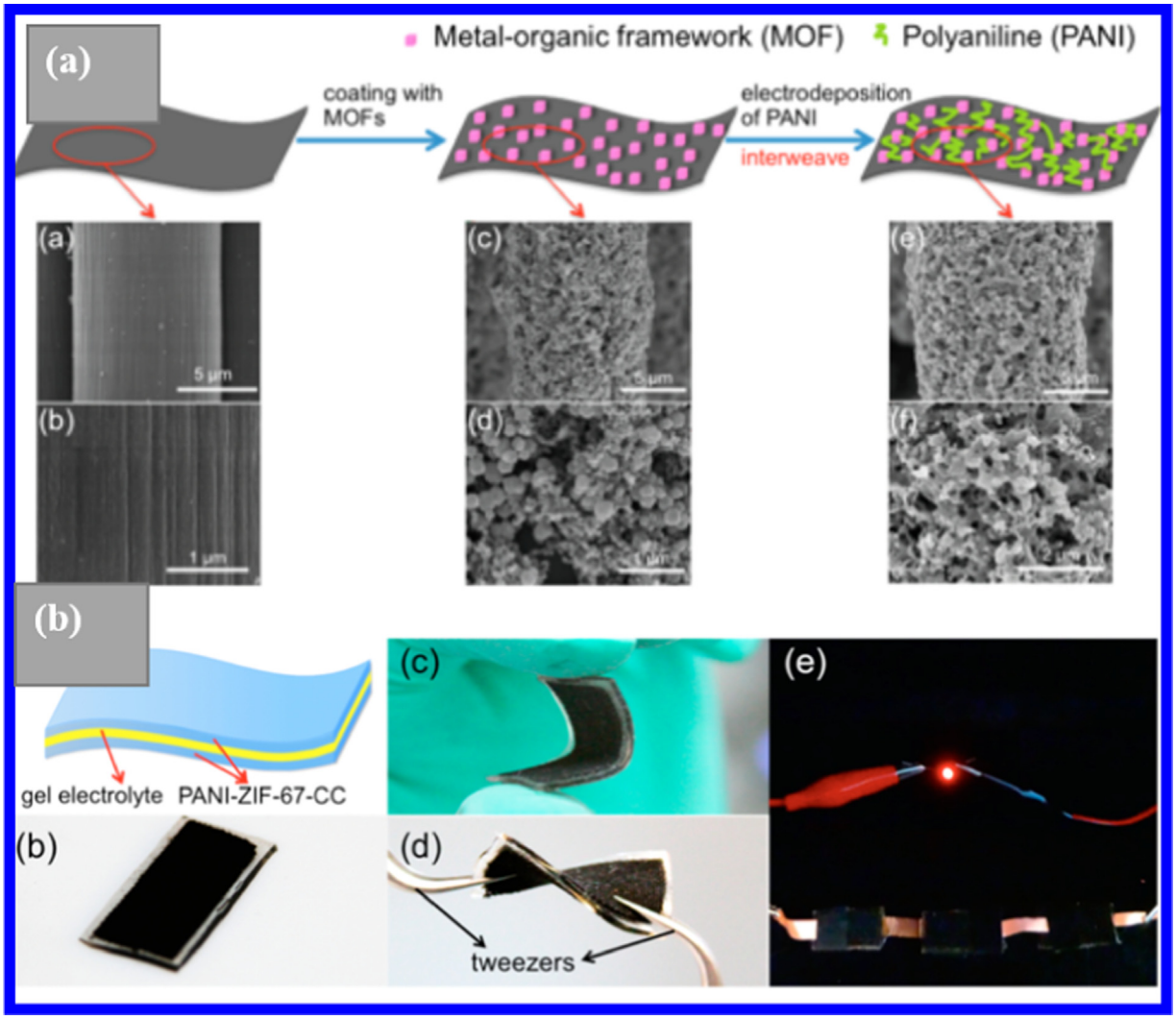

Fig. 23. (a) Schematic illustration of the two-step fabrication process of PANI-ZIF-67-CC electrodes and SEM images of the carbon cloth fibers, after coating with ZIF-67, and after electro-polymerization of aniline. (b) Schematic illustration of a PANI-ZIF-67-CC flexible solid-state supercapacitor device. Optical photographs of the fabricated flexible solid-state supercapacitor device under normal, bent, and twisted states. Photograph of a red LED powered by the three supercapacitors connected in series [159].

porous carbon and metal oxide or sulfide, which both treated as the electrode for EDLCs and pseudocapacitive. Three types of MOFs related nanomaterials, including MOFs, MOFs derived carbon and MOFs derived metal oxides, are summarized in Table 4 with different surface area and electrochemical performances.

Similar to their applications in LIBs, MOFs can also be used directly as electrode materials for supercapacitors due to their high surface area, porosity and large diversity of metal ions. In the early stages, Co8-MOF-5 ($Zn_{3.68}Co_{0.32}O(BDC)_3(DEF)_{0.75}$) was first reported as an electrode for EDLCs [153]. Subsequently, another Co-based MOF film was explored for supercapacitors with a good pseudocapacitive behavior with specific capacitance up to 206.76 F g^{-1}, as well as capacitance loss of only 1.5% after 1000 cycles [154].

Further research has been presented by the same group [155]. Three organic ligands with different molecular lengths were used to adjust the pore size of Co-based MOFs, in which the MOF with the longer organic linker ($[Co(bpdc)(H_2O)_2]H_2O$, bpdc=4,4-biphenyldicarboxylic acid) had larger pores, larger surface area, and highest capacitive properties. Enhancement of the electrochemical performance can be attributed to the continuously interconnected leaflet-like microstructure with fewer structural interfaces [155]. In another work, Wei's group firstly used a layered structure Ni-based MOF as an electrode material for supercapacitors with large specific capacitance, high rate capability of 1127 and 668 F g^{-1} at rates of 0.5 and 10 A g^{-1}, and cycling stability [156]. Very recently, another Zr-based MOF (UiO-66) has been synthesized under different reaction temperatures, resulting in different particle sizes and degrees of crystallization [157]. The sample obtained at low temperature (50 °C) had the smallest particle size and highest specific capacitance of 1144 F g^{-1} at a scan rate of 5 mV s^{-1}. Yaghi's group designed a series of 23 different MOFs with a variety of structure types, such as MOF-5, nNi-MOF-74, nHKUST-1, nMOF-177, nUiO-66, and nMOF-867. Among these, the zirconium MOF (nMOF-867) exhibited stack and areal capacitances of 0.64 and 5.09 mF cm^{-2}, about 6 times that of commercial activated carbon [158].

Due to the low conductivity of MOFs, an effective strategy was developed to interweave MOF crystals with conductive polyaniline (PANI) chains, shown in Fig. 23(a) [159]. The corresponding SEM images at each step of the coating process on carbon cloth fibers, after coating with ZIF-67 and after electro-polymerization of aniline, are shown as well. Interestingly, they further developed flexible solid-state supercapacitors using this PANI-ZIF-67-CC as electrodes and a gel electrolyte serving as a separator (as shown in Fig. 23(b)). They also used these devices to power small electronic devices, such as a light-emitting-diode (LED). These MOF-based solid-state supercapacitors show great potential for flexible and wearable electronics [159].

According to the above discussion, MOFs can be immediately used as the electrode materials for supercapacitors. With the rational design of metal ions, organic linkers, and reaction conditions, MOFs with controllable particle and pore sizes can achieve satisfactory electrochemical properties. However, the studies of MOFs directly in supercapacitors are still at an initial stage and more exploration is needed.

5.2. MOF-derived carbon for supercapacitors

In 2008, Xu's group first employed zinc-based MOF-5 as the template for nanoporous carbon to be used as an electrode material for EDLCs [160]. The as-synthesized nanoporous carbon exhibited a high surface area of 2872 m^2 g^{-1} and excellent electrochemical performance for an EDLC. The specific capacitance was maintained at 258 F g^{-1}, even at a current density of 250 mA g^{-1}. Further, the influence of the carbonizing temperature of MOF-5 from 530 to 1000 °C on the specific surface area, pore size distribution, and electrical conductivity were studied [161]. The porous carbon derived from MOF-5 at high temperatures demonstrated ideal electrochemical performance, owing to its high mesoporosity and good electrical conductivity. In their work, furfuryl alcohol was used as the carbon precursor introduced into the pores of MOF-5 by means of FA vapor. In another work, both phenolic resin, carbon tetrachloride, and ethylenediamine were chosen as the carbon precursors to adjust the texture and structure of MOF-5, resulting in different pore structures [33]. All the porous carbons were investigated in both aqueous and organic electrolytes for electrochemical performance. The as-developed mesoporous network carbons showed excellent performance and high capacitance retention ratios, with capacitances of 271 and 156 F g^{-1}, as well as gravimetric energy densities of 9.4 and 31.2 Wh kg^{-1} in aqueous and organic electrolytes, respectively.

Zeolite-type MOFs have also shown great potential for the synthesis of porous carbons [162–165]. Nanoporous carbon can be achieved through the direct carbonization of ZIF-8 at different temperatures [162,166]. With increasing annealing temperature, the surface area and micropore volume increases. When evaluating the electrochemical performance of the obtained samples in 0.5 M H_2SO_4 aqueous solutions, their capacitances were obviously enhanced with better carbonization at higher temperatures [166]. Another work selected furfuryl alcohol as the additional carbon source for ZIF-8, in which an unexpectedly high surface area of 3405 m^2 g^{-1} was achieved, along with good specific capacitances of ~200 F g^{-1} at a current density of 250 mA g^{-1} when used as an electrode material for EDLCs [167]. Additionally, different carbon sources, such as glucose, ethylene glycol, glycerol, and furfuryl alcohol, have been introduced into ZIF-7, in which the glucose modified ZIF-7 delivered the best specific capacitance (228 F g^{-1} at 0.1 A g^{-1}), high rate capability (178 F g^{-1} maintained at 10 A g^{-1}), and good cycling stability (94% capacitance retention over 5000 cycles) [168]. It was considered that the glucose-derived carbon helped to remove residual Zn impurities, prevent the formation of macropores, and create graphene-like structures that further contributed to the electrochemical performance [168]. Based on the importance of the pore's influence, some studies have focused on the design of the specific structure of porous carbon frameworks [169–171]. 3D hierarchical porous carbon frameworks with micro-, meso-, and macropores have been prepared by carbonization of ZIF-8 synthesized by ultrasonication [171]. In this case, the interconnected tiny pores within larger ones are beneficial to buffer ions in order to shorten the diffusion distances of the electrolyte to the interior surfaces, further enhancing ion mobility and charge storage [171]. Another similar result has been reported by Yu et al. [170]. The formation process of porous carbon with bimodal porosity is shown in Fig. 24(a) [170]. Silica colloids were embedded in the precursor and incorporated inside or between aggregated crystals. After an annealing process and removal of silica, mesopores were produced, along with the formation of micropores from intrinsic ZIF-8. The hierarchical porous carbon exhibits high capacitance, low resistance, and good capacitance retention (92–97%) after 2000 cycles.

In order to combine the properties of individual ZIF-8 and ZIF-67 MOFs, core–shell ZIF-8@ZIF-67 nanocomposites have been designed by applying a seed-mediated growth technique (Fig. 24(b)) [172]. The respective advantages and shortages of ZIF-8 and ZIF-67 are presented in Fig. 24(b). After thermal treatment of ZIF-8@ZIF-67 crystals, the authors obtained functionalized nanoporous hybrid carbon materials consisting of nitrogen-doped carbon (NC) as the cores from ZIF-8 and highly graphitic carbon (GC) as the shells from ZIF-67. As a result, the hybrid carbon material comines the advantageous properties of the individual NC and GC, exhibiting a specific capacitance of 270 F g^{-1}.

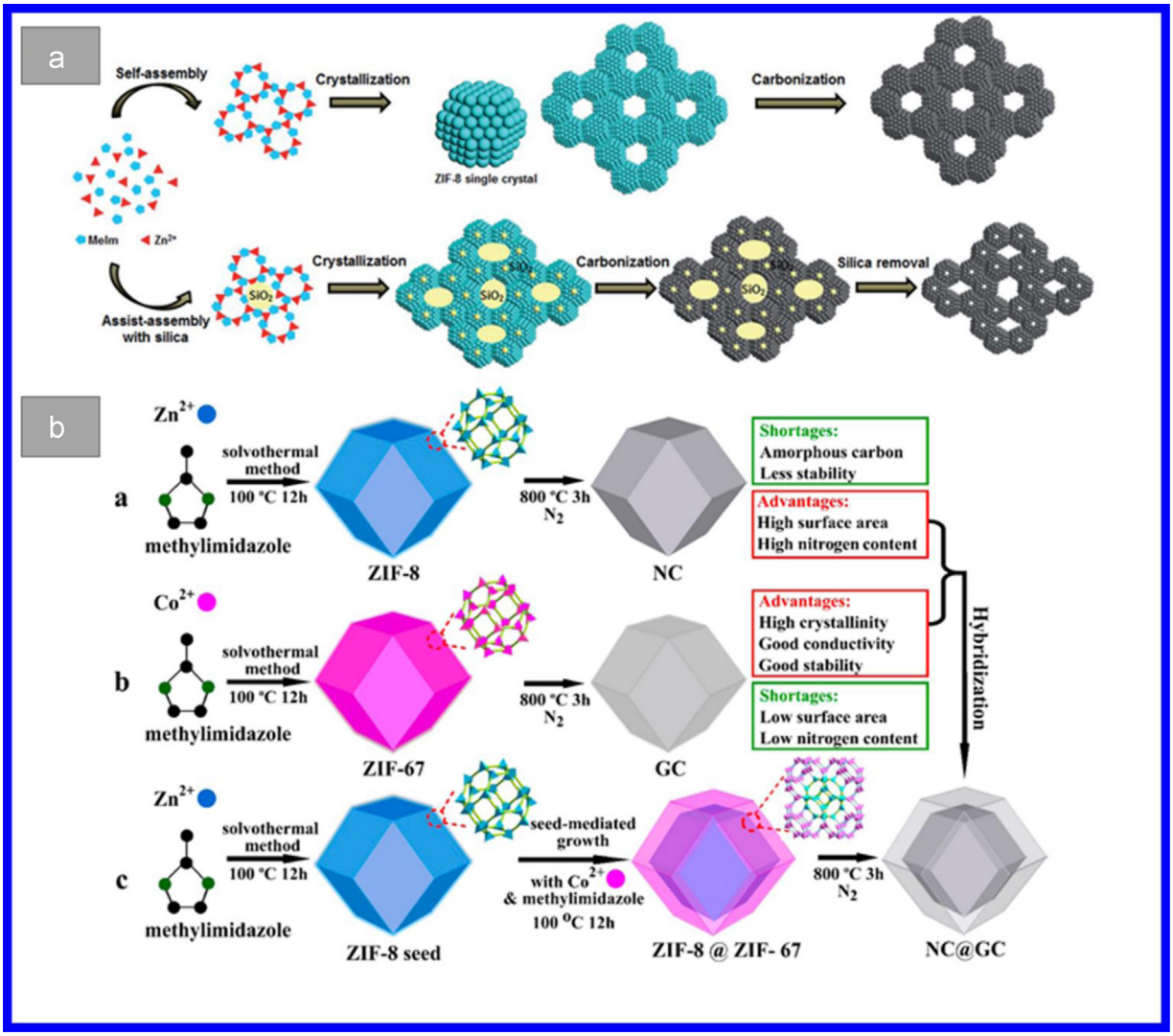

Fig. 24. (a) Formation process of porous carbons with bimodal porosity via self- and assisted-assembly approaches [170]. (b) Synthetic scheme for the preparation of ZIF-8 crystals and NC, ZIF-67 crystals and GC, and core–shell ZIF-8@ZIF-67 crystals and NC@GC [172].

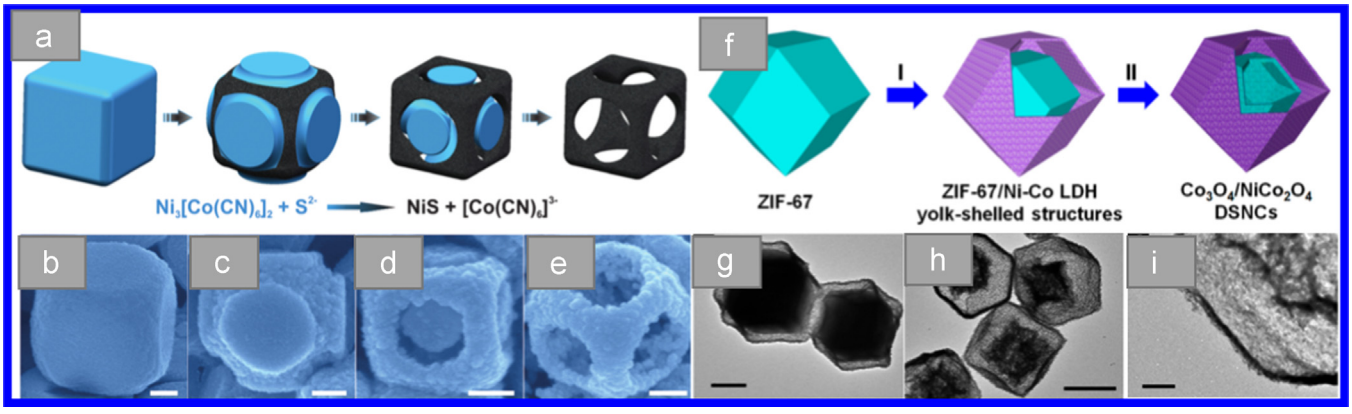

Fig. 25. (a) Schematic illustration of the formation process of NiS nanoframes. (b–e) FE-SEM images of the products obtained after reaction for (b) 0 h, (c) 0.5 h, (d) 2 h, and (e) 6 h. Scale bars: 100 nm [188]. (f) Schematic illustration of the formation process of $Co_3O_4/NiCo_2O_4$ DSNCs (g–i). TEM images of ZIF-67/Ni–Co LDH yolk-shelled structures (g), $Co_3O_4/NiCo_2O_4$ DSNCs (h, i) [192].

Besides the most popular Zn-based MOFs, other MOFs such as Al-based [173,174], Mg-based [173,175] and Cu-based [174] have also been investigated as precursors for porous carbons for supercapacitors.

5.3. MOF-derived metal oxides for supercapacitors

Generally, metal oxides always have higher capacitance and energy density than those of conventional carbon materials as

pesudocapacitors [176,177]. Various kinds of metal oxides, such as MnO_2, Co_3O_4, NiO, and V_2O_5, have been studied as electrode materials for supercapacitors. The requirements of ideal metal oxide electrode materials can be summarized as follows: (1) high surface area; (2) controlled porosity; (3) high electronic conductivity; and (4) high thermal and chemical stability [178]. Based on these requirements, MOFs show great promise as precursors or templates for the manufacture of metal oxides. For example, a kind of porous Co_3O_4 was obtained by the simple thermolysis of Co-MOF crystals ($(((Co_3(abtc)_3(bpy)_{1.5}(H_2O)_3)(H_2O)_2)_n$) [179]. The as-prepared Co_3O_4 particles displayed well-defined porous features with high specific capacitance and slightly enhanced capacitance after 3400 cycles when investigated in 2 M KOH electrolyte. The popular ZIF-67 has also been used as the precursor for preparing hollow rhombic dodecahedral Co_3O_4, which showed a large specific capacitance of 1100 F g^{-1} and excellent stability of 95.1% of the specific capacitance after 6000 charge–discharge cycles [180]. In this case, the high specific surface area, porosity, and specific structural features inherited from the MOF precursors made great contributions to the enhanced electrochemical performance. except of Co_3O_4, CeO_2 derived from Ce-MOFs has been reported as the electrode for pseudocapacitors as well [181]. Furthermore, MTMOs synthesized from MOFs can also be used as the electrodes for supercapacitors. Qiu et al. prepared porous $ZnCo_2O_4$ nanoparticles from zinc and cobalt mixed-MOFs (JUC-155) with an exceptionally high specific capacitance of 451 F g^{-1} at a scan rate of 5 mV s^{-1} and excellent cycling stability [182].

Due to the expectation of high conductivity, one general approach is to retain the carbon layers decomposed from the organic linkers during the annealing [183]. In a typical process, porous Fe_3O_4/carbon composites were prepared via a facile one-step calcination of Fe-MOFs [184]. Two other kinds of Cr_2O_3/carbon and Ni/carbon composites were subsequently synthesized via a similar annealing process of Cr-MOFs and Ni-MOFs, respectively [185,186]. As a result, the as-prepared metal/carbon composites obtained the high specific capacitance and long term cycling stability attributed to the porous structure, as well as the good conductivity from the retained carbon. Very recently, a novel MOF-templated sulfidation method has been developed to synthesize $Cu_{1.96}S$/carbon hybrids, in which the copper sulfide nanoparticles are embedded within a porous carbon matrix [187]. With increasing annealing temperatures, the composites have increasing surface areas and carbon content, resulting in increased specific capacitance and stability, which is related to the increased extent of the carbonization [187].

Recently, a novel kind of NiS nanoframe with tunable size was synthesized by an anisotropic chemical etching/anion exchange method [188]. A schematic illustration of the formation process and corresponding SEM images at different stages are shown in Fig. 25(a) and (b–e), respectively. In this process, the different reactivity between the edges and the plane surface of the Ni–Co PBA nanocubes is the key factor for the formation of NiS nanoframes. The as-prepared NiS nanoframes can maintain a high capacitance of 1290 F g^{-1} (91.8% retention) after 4000 cycles, benefitting from their structural merits, including a 3D open structure, small primary nanoparticle size, high specific surface area, and good structural robustness. Furthermore, the hierarchical nano/micro-structures have great potential for use in supercapacitors due to their high surface/body ratios, large surface areas, better permeability, and more surface active sites [189,190]. MOFs are a good choice for the fabrication of hierarchical nano/micro-structures with various unique properties. Chen et al. designed layered double hydroxide (LDHs) hollow nano-polyhedra with a ZIF-67 template to obtain Ni–Co and Mg–Co LDH nanocages. When investigating the electrochemical properties in KOH electrolyte, the Ni–Co LDH nanocages exhibited superior pseudocapacitance properties due to their novel hierarchical and submicroscopic structures [191]. In another work, similar Ni-Co LDH nanocages were prepared and subsequently annealed to achieve $Co_3O_4/NiCo_2O_4$ double-shelled nanocages [192]. The schematic illustration of the whole formation process is shown in Fig. 25(f), with the SEM images of Ni–Co LDH nanocages and $Co_3O_4/NiCo_2O_4$ double-shelled nanocages in Fig. 25(g) and (h, i), respectively. The $Co_3O_4/NiCo_2O_4$ double-shelled nanocages exhibited a high specific capacitance of 972 F g^{-1} and excellent stability, lasting for 12000 cycles as an electrode for pseudocapacitors, superior to that of Co_3O_4 nanocages and Co_3O_4/Co_3O_4 double-shelled nanocages.

5.4. Summary and perspectives

In this section, the potential application of MOFs in supercapacitors has been summarized in detail (Table 3). MOFs with controllable particle and pore sizes can be directly used as electrode materials for supercapacitors. The electrochemical performances of MOFs in supercapacitors are quite superior and stable. However, efforts should be further attempted to develop more kinds of MOFs for this application. Secondly, MOFs are treated as excellent templates and precursors for the development of porous carbons and metal oxides. The as-prepared porous carbons and metal oxide inherit the high surface area and porosity from their precursor MOFs, which demonstrates the great potential for their applications in EDLCs and pseudocapacitors. More interestingly, due to the unique structures and morphology of MOFs, they can be used to design and fabricate hierarchical nanostructured metal oxides or MTMOs. In this case, advantages from different MOFs can be combined, leading to even better properties for supercapacitors. Thus, MOFs and MOF-based materials can be promising alternatives electrodes for EDLCs and pseudocapacitors, especially as precursors for the design of hierarchical nanostructured materials.

6. Outlook and perspective

MOFs, as a novel family of porous crystalline materials, exhibit a wide range of applications, especially in the field of energy storage and conversion including fuel cells, batteries and supercapacitors. In this review, we summarized the recent developments and understanding of MOFs and MOF-derived nanomaterials, as well as their applications in clean energy.

Firstly, MOFs can be directly used as the electrocatalysts in fuel cells and electrodes in batteries and supercapacitors. Their unique advantages, including high surface area, high porosity, adjustable pore size, and controllable structure make great contributions to their electrochemical performance. However, the perform of MOFs in most of these applications are not yet satisfactory. A common issue for MOFs is their limited electronic conductivity due to the existence of organic linkers. With further research, high conductivity MOFs are expected to be developed and used in electrochemical devices.

Secondly, MOF-derived porous carbons, metal oxides, and metal sulfides can also be adopted for use in fuel cells, batteries, and supercapacitors. Because of the organic ligands and metal ions inside MOFs, they are an excellent choice as precursors and templates for the synthesis of the abovementioned materials with different nanostructures. In general, as-prepared porous carbons and metal oxides inherit the major advantages of the precursor MOFs, resulting in improved electrochemical performance compared to other nanomaterials synthesized from other methods. For further performance enhancement of porous carbon-derived MOFs, heteroatom doping such as N, S and P, is an effective

approach, and can be achieved either during the manufacturing of MOFs or at the post-processing stage. However, controlling these species and the ratio of heteroatoms is still a major challenge. Research is currently focused more on fabricating the nanostructured materials of metal oxides and their composites derived from MOFs. In addition, mixed transition-metal oxides have also attracted more attention due to their wide range of applications, and can be obtained from MOFs using a simple approach.

Thirdly, it is a trend to design and build novel hierarchical nanostructures by MOFs. Obviously, complementary properties can be realized from different MOFs, which lead to superior performance based on controllable shape, particle size, crystal structure, and purity.

In conclusion, MOFs and MOF-derived nanomaterials show great potential in the field of energy storage and conversion due to their unique properties. Nonetheless, there are still issues and room for improvement in both the synthesis and pyrolysis processes of MOFs. On one hand, purposive fabrication of highly electrically conductive MOFs is a big challenge when directly applied to MOFs for energy storage and conversion. On the other hand, for MOFs derived porous carbon or metal oxide composites, manufacture of controllable structure and morphology are still ongoing, in which the uniform distribution between metal particles and carbon matrix is still not very easily to obtain. Meanwhile, the bonding effect, component proportional, and particle distribution of metal particles and carbon in the MOFs derived composites through post-treatment is still calling for deeper understanding. Another important issue that should be pointed out is to create an effective method to mass produce both MOFs and MOF-derived materials in large scale, which can lead the fast development of MOFs in practical applications for energy storage and conversion.

Acknowledgments

This research was supported by the Natural Science and Engineering Research Council of Canada (NSERC), the Canada Research Chair Program (CRC), the Canada Foundation for Innovation (CFI), and the University of Western Ontario (UWO).

References

[1] M.C. Das, et al., Functional Mixed metal–organic frameworks with metalloligands, Angew. Chem. Int. Ed. 50 (45) (2011) 10510–10520.
[2] H. Furukawa, et al., The chemistry and applications of metal-organic frameworks, Science 341 (2013) 6149.
[3] W. Lu, et al., Tuning the structure and function of metal-organic frameworks via linker design, Chem. Soc. Rev. 43 (16) (2014) 5561–5593.
[4] N. Stock, S. Biswas, Synthesis of metal-organic frameworks (MOFs): routes to various MOF topologies, morphologies, and composites, Chem. Rev., 112, (2012) 933–969.
[5] H.-C. Zhou, J.R. Long, O.M. Yaghi, Introduction to metal–organic frameworks, Chem. Rev. 112 (2) (2012) 673–674.
[6] H. Furukawa, O.M. Yaghi, Storage of hydrogen, methane, and carbon dioxide in highly porous covalent organic frameworks for clean energy applications, J. Am. Chem. Soc. 131 (25) (2009) 8875–8883.
[7] H. Furukawa, et al., Ultrahigh porosity in metal-organic frameworks, Science 329 (5990) (2010) 424–428.
[8] O.K. Farha, et al., Designing higher surface area metal–organic frameworks: Are triple bonds better than phenyls? J. Am. Chem. Soc. 134 (24) (2012) 9860–9863.
[9] H. Deng, et al., Large-pore apertures in a series of metal-organic frameworks, Science 336 (6084) (2012) 1018–1023.
[10] N.W. Ockwig, et al., Reticular chemistry: occurrence and taxonomy of nets and grammar for the design of frameworks, Acc. Chem. Res. 38 (3) (2005) 176–182.
[11] Y. Cui, et al., A luminescent mixed-lanthanide metal–organic framework thermometer, J. Am. Chem. Soc. 134 (9) (2012) 3979–3982.
[12] X. Kong, et al., CO_2 dynamics in a metal–organic framework with open metal sites, J. Am. Chem. Soc. 134 (35) (2012) 14341–14344.
[13] C. Dey, T. Kundu, R. Banerjee, Reversible phase transformation in proton conducting Strandberg-type POM based metal organic material, Chem. Commun. 48 (2) (2012) 266–268.
[14] A.M. Shultz, et al., A catalytically active, permanently microporous MOF with metalloporphyrin struts, J. Am. Chem. Soc. 131 (12) (2009) 4204–4205.
[15] V. Stavila, et al., Reversible hydrogen storage by $NaAlH_4$ confined within a titanium-functionalized MOF-74(Mg) nanoreactor, ACS Nano 6 (11) (2012) 9807–9817.
[16] C. Dey, T.K., B.P. Biswal, A. Mallick, R. Banerjee, Crystalline metal-organic frameworks (MOFs): synthesis, structure and function. Acta Cryst. (2014) B70, 3–10.
[17] S.-L. Li, Q. Xu, Metal–organic frameworks as platforms for clean energy, Energy Environ. Sci. 6 (6) (2013) 1656.
[18] Y.-R. Lee, J. Kim, W.-S. Ahn, Synthesis of metal-organic frameworks: a mini review, Korean J. Chem. Eng. 30 (9) (2013) 1667–1680.
[19] Z. Ni, R.I. Masel, Rapid production of metal−organic frameworks via microwave-assisted solvothermal synthesis, J. Am. Chem. Soc. 128 (38) (2006) 12394–12395.
[20] N.A. Khan, E. Haque, S.H. Jhung, Rapid syntheses of a metal-organic framework material $Cu_3(BTC)_2(H_2O)_3$ under microwave: a quantitative analysis of accelerated syntheses, Phys. Chem. Chem. Phys. 12 (11) (2010) 2625–2631.
[21] E. Haque, et al., Synthesis of a metal–organic framework material, iron terephthalate, by ultrasound, microwave, and conventional electric heating: a kinetic study, Chem. – Eur. J. 16 (3) (2010) 1046–1052.
[22] J. Kim, et al., Control of catenation in CuTATB-n metal-organic frameworks by sonochemical synthesis and its effect on CO_2 adsorption, J. Mater. Chem. 21 (9) (2011) 3070–3076.
[23] M. Hartmann, et al., Adsorptive separation of isobutene and isobutane on $Cu_3(BTC)_2$, Langmuir 24 (16) (2008) 8634–8642.
[24] T. Friščić, et al., Ion- and liquid-assisted grinding: improved mechanochemical synthesis of metal–organic frameworks reveals salt inclusion and anion templating, Angew. Chem. Int. Ed. 49 (4) (2010) 712–715.
[25] P. Cubillas, M.W. Anderson, M.P. Attfield, Influence of isomorphous substituting cobalt ions on the crystal growth of the MOF-5 framework determined by atomic force microscopy of growing core–shell crystals, Cryst. Growth Des. 13 (10) (2013) 4526–4532.
[26] P.Y. Moh, et al., Revelation of the molecular assembly of the nanoporous metal organic framework ZIF-8, J. Am. Chem. Soc. 133 (34) (2011) 13304–13307.
[27] C. Zheng, et al., Microstructural study of the formation mechanism of metal-organic framework MOF-5, CrystEngComm 16 (6) (2014) 1064–1070.
[28] S.J. Yang, et al., MOF-derived hierarchically porous carbon with exceptional porosity and hydrogen storage capacity, Chem. Mater. 24 (3) (2012) 464–470.
[29] Y. Meng, et al., Crystal-like microporous hybrid solid nanocast from Cr-MIL-101, Chem. Commun. 47 (37) (2011) 10479–10481.
[30] M. Hu, et al., Direct carbonization of Al-based porous coordination polymer for synthesis of nanoporous carbon, J. Am. Chem. Soc. 134 (6) (2012) 2864–2867.
[31] L. Radhakrishnan, et al., Preparation of microporous carbon fibers through carbonization of Al-based porous coordination polymer (Al-PCP) with furfuryl alcohol, Chem. Mater. 23 (5) (2011) 1225–1231.
[32] D. Yuan, et al., Worm-like mesoporous carbon synthesized from metal–organic coordination polymers for supercapacitors, Electrochem. Commun. 11 (6) (2009) 1191–1194.
[33] J. Hu, et al., Porous carbons prepared by using metal–organic framework as the precursor for supercapacitors, Carbon 48 (12) (2010) 3599–3606.
[34] H.-L. Jiang, et al., From metal–organic framework to nanoporous carbon: toward a very high surface area and hydrogen uptake, J. Am. Chem. Soc. 133 (31) (2011) 11854–11857.
[35] X. Xu, et al., Spindle-like mesoporous α-Fe_2O_3 anode material prepared from MOF template for high-rate lithium batteries, Nano Lett. 12 (9) (2012) 4988–4991.
[36] S. Ma, et al., Cobalt imidazolate framework as precursor for oxygen reduction reaction electrocatalysts, Chem. – Eur. J. 17 (7) (2011) 2063–2067.
[37] C. Laberty-Robert, et al., Design and properties of functional hybrid organic–inorganic membranes for fuel cells, Chem. Soc. Rev. 40 (2) (2011) 961–1005.
[38] M.K. Debe, Electrocatalyst approaches and challenges for automotive fuel cells, Nature 486 (7401) (2012) 43–51.
[39] B.G. Pollet, I. Staffell, J.L. Shang, Current status of hybrid, battery and fuel cell electric vehicles: from electrochemistry to market prospects, Electrochim. Acta 84 (2012) 235–249.
[40] D. Papageorgopoulos, DOE hydrogen and fuel cells program, VFY 2013 Annual Progress Report, 2013.
[41] D. Banham, et al., A review of the stability and durability of non-precious metal catalysts for the oxygen reduction reaction in proton exchange membrane fuel cells, J. Power Sources 285 (2015) 334–348.
[42] Y. Wang, et al., A review of polymer electrolyte membrane fuel cells: technology, applications, and needs on fundamental research, Appl. Energy 88 (4) (2011) 981–1007.
[43] J. Wu, H. Yang, Platinum-based oxygen reduction electrocatalysts, Acc. Chem. Res. 46 (8) (2013) 1848–1857.
[44] N. Cheng, et al., Extremely stable platinum nanoparticles encapsulated in a zirconia nanocage by area-selective atomic layer deposition for the oxygen reduction reaction, Adv. Mater. 27 (2) (2015) 277–281.

[45] N. Cheng, et al., Atomic scale enhancement of metal-support interactions between Pt and ZrC for highly stable electrocatalysts, Energy Environ. Sci. 8 (5) (2015) 1450–1455.
[46] J. Mao, Electrocatalytic four-electron reduction of oxygen with Copper (II)-based metal-organic frameworks, Electrochem. Commun. 19 (2012) 29–31.
[47] M. Jahan, Z. Liu, K.P. Loh, A graphene oxide and copper-centered metal organic framework composite as a tri-functional catalyst for HER, OER, and ORR, Adv. Funct. Mater. 23 (43) (2013) 5363–5372.
[48] M. Jahan, Q. Bao, K.P. Loh, Electrocatalytically active graphene–porphyrin MOF composite for oxygen reduction reaction, J. Am. Chem. Soc. 134 (15) (2012) 6707–6713.
[49] L. Zhang, et al., Highly graphitized nitrogen-doped porous carbon nanopolyhedra derived from ZIF-8 nanocrystals as efficient electrocatalysts for oxygen reduction reactions, Nanoscale 6 (12) (2014) 6590–6602.
[50] X. Zhao, et al., One-step synthesis of nitrogen-doped microporous carbon materials as metal-free electrocatalysts for oxygen reduction reaction, J. Mater. Chem. A 2 (30) (2014) 11666–11671.
[51] P. Zhang, et al., ZIF-derived in situ nitrogen-doped porous carbons as efficient metal-free electrocatalysts for oxygen reduction reaction, Energy Environ. Sci. 7 (1) (2014) 442–450.
[52] J. Li, et al., Metal-organic framework templated nitrogen and sulfur co-doped porous carbons as highly efficient metal-free electrocatalysts for oxygen reduction reactions, J. Mater. Chem. A 2 (18) (2014) 6316–6319.
[53] M. Yoon, D. Moon, New Zr (IV) based metal-organic framework comprising a sulfur-containing ligand: enhancement of CO_2 and H_2 storage capacity, Microporous Mesoporous Mater. 215 (2015) 116–122.
[54] J. Yoo, et al., Homogeneous decoration of zeolitic imidazolate framework-8 (ZIF-8) with core-shell structures on carbon nanotubes, RSC Adv. 4 (91) (2014) 49614–49619.
[55] L. Ge, et al., High activity electrocatalysts from metal–organic framework-carbon nanotube templates for the oxygen reduction reaction, Carbon 82 (0) (2015) 417–424.
[56] J. Wei, et al., Nitrogen-doped nanoporous carbon/graphene nano-sandwiches: synthesis and application for efficient oxygen reduction, Adv. Funct. Mater. 25 (36) (2015) 5768–5777.
[57] X. Wang, et al., MOF derived catalysts for electrochemical oxygen reduction, J. Mater. Chem. A 2 (34) (2014) 14064–14070.
[58] W. Xia, et al., Well-defined carbon polyhedrons prepared from nano metal-organic frameworks for oxygen reduction, J. Mater. Chem. A 2 (30) (2014) 11606–11613.
[59] S. Zhao, et al., Carbonized nanoscale metal–organic frameworks as high performance electrocatalyst for oxygen reduction reaction, ACS Nano 8 (12) (2014) 12660–12668.
[60] F. Afsahi, S. Kaliaguine, Non-precious electrocatalysts synthesized from metal-organic frameworks, J. Mater. Chem. A 2 (31) (2014) 12270–12279.
[61] E. Proietti, et al., Iron-based cathode catalyst with enhanced power density in polymer electrolyte membrane fuel cells, Nat. Commun. 2 (2011) 416.
[62] J.-S. Li, et al., Nitrogen-doped Fe/Fe_3C@graphitic layer/carbon nanotube hybrids derived from MOFs: efficient bifunctional electrocatalysts for ORR and OER, Chem. Commun. 51 (13) (2015) 2710–2713.
[63] W. Xia, et al., A metal-organic framework route to in situ encapsulation of Co@Co3O4@C core@bishell nanoparticles into a highly ordered porous carbon matrix for oxygen reduction, Energy Environ. Sci. 8 (2) (2015) 568–576.
[64] Y. Hou, et al., An advanced nitrogen-doped graphene/cobalt-embedded porous carbon polyhedron hybrid for efficient catalysis of oxygen reduction and water splitting, Adv. Funct. Mater. 25 (6) (2015) 872–882.
[65] M.S. Islam, C.A. Fisher, Lithium and sodium battery cathode materials: computational insights into voltage, diffusion and nanostructural properties, Chem. Soc. Rev. 43 (1) (2014) 185–204.
[66] G. Ferey, et al., Mixed-valence Li/Fe-based metal-organic frameworks with both reversible redox and sorption properties, Angew. Chem. Int. Ed. Engl. 46 (18) (2007) 3259–3263.
[67] Gd Combarieu, et al., In situ Fe XAFS of reversible lithium insertion in a flexible metal organic framework material, Electrochem. Commun. 11 (10) (2009) 1881–1884.
[68] C. Combelles, M.B.Y.L. Pedesseau, M.-L. Doublet, Design of electrode materials for lithium-ion batteries: the example of metal-organic frameworks, J. Phys. C.hem. C. 114 (2010) 9518–9527.
[69] C. Combelles, et al., FeII/FeIII mixed-valence state induced by Li-insertion into the metal-organic-framework Mil53(Fe): A DFT+U study, J. Power Sources 196 (7) (2011) 3426–3432.
[70] G. de Combarieu, M.M.F. Millange, N. Guillou, J. Cabana, C. Grey, I. Margiolaki, G. Fe´rey, J.-M. Tarascon, Influence of the benzoquinone sorption on the structure and electrochemical performance of the MIL-53(Fe) hybrid porous material in a lithium-ion battery, Chem. Mater. 21 (2009) 1602–1611.
[71] A. Fateeva, et al., Synthesis, structure, characterization, and redox properties of the porous MIL-68(Fe) solid, Eur. J. Inorg. Chem. 2010 (24) (2010) 3789–3794.
[72] J. Shin, et al., MIL-101(Fe) as a lithium-ion battery electrode material: a relaxation and intercalation mechanism during lithium insertion, J. Mater. Chem. A 3 (8) (2015) 4738–4744.
[73] A. Shahul Hameed, et al., A layered oxalatophosphate framework as a cathode material for Li-ion batteries, J. Mater. Chem. A 1 (18) (2013) 5721.
[74] X. Li, et al., Shape-controlled synthesis and lithium-storage study of metal-organic frameworks Zn_4O(1,3,5-benzenetribenzoate)$_2$, J. Power Sources 160 (1) (2006) 542–547.
[75] K. Saravanan, et al., Lithium storage in a metal organic framework with diamondoid topology – a case study on metal formates, J. Mater. Chem. 20 (38) (2010) 8329.
[76] L. Gou, et al., One-pot synthesis of a metal–organic framework as an anode for Li-ion batteries with improved capacity and cycling stability, J. Solid State Chem. 210 (1) (2014) 121–124.
[77] P.C. Cheng, et al., Synthesis, structures, and properties of alkali and alkaline earth coordination polymers based on V-shaped ligand, CrystEngComm 14 (20) (2012) 6812.
[78] P. Nie, et al., Prussian blue analogues: a new class of anode materials for lithium ion batteries, J. Mater. Chem. A 2 (16) (2014) 5852.
[79] Y. Lin, et al., An exceptionally stable functionalized metal-organic framework for lithium storage, Chem. Commun. 51 (4) (2015) 697–699.
[80] X. Zheng, et al., Metal–organic frameworks: promising materials for enhancing electrochemical properties of nanostructured Zn_2SnO_4 anode in Li-ion batteries, CrystEngComm 14 (6) (2012) 2112.
[81] Y. Han, et al., In situ growth of MOFs on the surface of si nanoparticles for highly efficient lithium storage: Si@MOF nanocomposites as anode materials for lithium-ion batteries, ACS Appl. Mater. Interfaces 7 (4) (2015) 2178–2182.
[82] Y. Zhao, et al., Significant impact of 2D graphene nanosheets on large volume change tin-based anodes in lithium-ion batteries: a review, J. Power Sources 274 (2015) 869–884.
[83] F. Zheng, Y. Yang, Q. Chen, High lithium anodic performance of highly nitrogen-doped porous carbon prepared from a metal-organic framework, Nat. Commun. 5 (2014) 5261.
[84] Q. Qu, et al., MOF-derived microporous carbon as a better choice for Na-ion batteries than mesoporous CMK-3, RSC Adv. 4 (110) (2014) 64692–64697.
[85] B. Liu, et al., Converting cobalt oxide subunits in cobalt metal-organic framework into agglomerated Co_3O_4 nanoparticles as an electrode material for lithium ion battery, J. Power Sources 195 (3) (2010) 857–861.
[86] C. Li, et al., Mesoporous nanostructured Co O derived from MOF template: a high-performance anode material for lithium-ion batteries, J. Mater. Chem. A 3 (10) (2015) 5585–5591.
[87] B. Yan, et al., Co_3O_4 nanostructures with a high rate performance as anode materials for lithium-ion batteries, prepared via book-like cobalt–organic frameworks, CrystEngComm 16 (44) (2014) 10227–10234.
[88] J. Guo, et al., Topochemical transformation of Co(ii) coordination polymers to Co_3O_4 nanoplates for high-performance lithium storage, J. Mater. Chem. A 3 (5) (2015) 2251–2257.
[89] K.J. Lee, et al., Preparation of Co_3O_4 electrode materials with different microstructures via pseudomorphic conversion of Co-based metal–organic frameworks, J. Mater. Chem. A 2 (35) (2014) 14393.
[90] R. Wu, et al., Zeolitic imidazolate framework 67-derived high symmetric porous Co(3)O(4) hollow dodecahedra with highly enhanced lithium storage capability, Small 10 (10) (2014) 1932–1938.
[91] P. Su, et al., Enhanced lithium storage capacity of Co3O4hexagonal nanorings derived from Co-based metal organic frameworks, J. Mater. Chem. A 2 (41) (2014) 17408–17414.
[92] A. Banerjee, et al., Superior lithium storage properties of α-Fe_2O_3 nano-assembled spindles, Nano Energy 2 (5) (2013) 890–896.
[93] X. Xu, et al., Spindle-like mesoporous alpha-Fe(2)O(3) anode material prepared from MOF template for high-rate lithium batteries, Nano Lett. 12 (9) (2012) 4988–4991.
[94] L. Zhang, et al., Formation of Fe_2O_3 microboxes with hierarchical shell structures from metal-organic frameworks and their lithium storage properties, J. Am. Chem. Soc. 134 (42) (2012) 17388–17391.
[95] L. Zhang, et al., Porous Fe_2O_3 nanocubes derived from MOFs for highly reversible lithium storage, CrystEngComm 15 (45) (2013) 9332.
[96] R. Wu, et al., MOF-templated formation of porous CuO hollow octahedra for lithium-ion battery anode materials, J. Mater. Chem. A 1 (37) (2013) 11126.
[97] A. Banerjee, et al., Synthesis of CuO nanostructures from Cu-based metal organic framework (MOF-199) for application as anode for Li-ion batteries, Nano Energy 2 (6) (2013) 1158–1163.
[98] Z. Wang, et al., Porous anatase TiO_2 constructed from a metal–organic framework for advanced lithium-ion battery anodes, J. Mater. Chem. A 2 (31) (2014) 12571.
[99] Y. Tan, et al., N-doped graphene/Fe–Fe_3C nano-composite synthesized by a Fe-based metal organic framework and its anode performance in lithium ion batteries, Chem. Eng. J. 258 (2014) 93–100.
[100] M. Li, et al., Large-scale fabrication of porous carbon-decorated iron oxide microcuboids from Fe–MOF as high-performance anode materials for lithium-ion batteries, RSC Adv. 5 (10) (2015) 7356–7362.
[101] S.J. Yang, et al., Preparation and exceptional lithium anodic performance of porous carbon-coated ZnO quantum dots derived from a metal-organic framework, J. Am. Chem. Soc. 135 (20) (2013) 7394–7397.
[102] H. Yue, et al., MOF-derived cobalt-doped ZnO@C composites as a high-performance anode material for lithium-ion batteries, ACS Appl. Mater. Interfaces 6 (19) (2014) 17067–17074.
[103] K. Shiva, et al., In-situ stabilization of tin nanoparticles in porous carbon matrix derived from metal organic framework: high capacity and high rate capability anodes for lithium-ion batteries, Z. Anorg. Allg. Chem. 640 (6) (2014) 1115–1118.
[104] Z. Wang, et al., Highly dispersed β-NiS nanoparticles in porous carbon matrices by a template metal–organic framework method for lithium-ion cathode, J. Mater. Chem. A 2 (21) (2014) 7912.

[105] C. Yuan, et al., Mixed transition-metal oxides: design, synthesis, and energy-related applications, Angew. Chem. Int. Ed. Engl. 53 (6) (2014) 1488–1504.
[106] J. Zhao, et al., Spinel $ZnMn_2O_4$ nanoplate assemblies fabricated via "escape-by-crafty-scheme" strategy, J. Mater. Chem. 22 (26) (2012) 13328.
[107] H. Guo, et al., General design of hollow porous $CoFe_2O_4$ nanocubes from metal-organic frameworks with extraordinary lithium storage, Nanoscale 6 (24) (2014) 15168–15174.
[108] F. Zheng, et al., Metal–organic framework-derived porous $Mn_{1.8}Fe_{1.2}O_4$ nanocubes with an interconnected channel structure as high-performance anodes for lithium ion batteries, J. Mater. Chem. A 3 (6) (2015) 2815–2824.
[109] Wu, X.Q. Renbing, Kun Zhou, Jun Wei, Jun Lou, Pulickel M. Ajayan, Porous Spinel $Zn_xCo_{3-x}O_4$ hollow polyhedra templated for high-rate lithium-ion batteries, ACS Nano 8 (2014) 6297–6303.
[110] G. Huang, et al., Core–shell $NiFe_2O_4$@TiO_2 nanorods: an anode material with enhanced electrochemical performance for lithium-ion batteries, Chemistry 20 (35) (2014) 11214–11219.
[111] G. Huang, et al., Hierarchical $NiFe_2O_4/Fe_2O_3$ nanotubes derived from metal organic frameworks for superior lithium ion battery anodes, J. Mater. Chem. A 2 (21) (2014) 8048.
[112] F. Zou, et al., MOF-derived porous ZnO/ZnFe(2)O(4)/C octahedra with hollow interiors for high-rate lithium-ion batteries, Adv. Mater. 26 (38) (2014) 6622–6628.
[113] Chencheng Sun, J.Y. Xianhong Rui, Weina Zhang, Qingyu Yan, Peng Chen, Fengwei Huo, Wei Huang, Xiaochen Dong, MOF-directed templating synthesis of porous multicomponent dodecahedron with hollow interiors for enhanced lithium-ion battery anodes, J. Mater. Chem. A (2015).
[114] Z. Guo, et al., Electrochemical performance of graphene and copper oxide composites synthesized from a metal–organic framework (Cu-MOF), RSC Adv. 3 (41) (2013) 19051.
[115] L. Hu, et al., CuO/Cu_2O composite hollow polyhedrons fabricated from metal-organic framework templates for lithium-ion battery anodes with a long cycling life, Nanoscale 5 (10) (2013) 4186–4190.
[116] Z. Li, et al., Prussion blue-supported annealing chemical reaction route synthesized double-shelled Fe(2)O(3)/Co(3)O(4) hollow microcubes as anode materials for lithium-ion battery, ACS Appl. Mater. Interfaces 6 (11) (2014) 8098–8107.
[117] B. Wang, et al., Cr_2O_3@TiO_2 yolk/shell octahedrons derived from a metal–organic framework for high-performance lithium-ion batteries, Microporous Mesoporous Mater. 203 (2015) 86–90.
[118] J. Wu, et al., Zn–Fe–ZIF-derived porous $ZnFe_2O_4$/C@NCNT nanocomposites as anodes for lithium-ion batteries, J. Mater. Chem. A (2015).
[119] Y. Han, et al., A novel anode material derived from organic-coated ZIF-8 nanocomposites with high performance in lithium ion batteries, Chem. Commun. 50 (59) (2014) 8057–8060.
[120] L. Zhang, H.B. Wu, X.W. Lou, Metal-organic-frameworks-derived general formation of hollow structures with high complexity, J. Am. Chem. Soc. 135 (29) (2013) 10664–10672.
[121] L. Hu, Q. Chen, Hollow/porous nanostructures derived from nanoscale metal-organic frameworks towards high performance anodes for lithium-ion batteries, Nanoscale 6 (3) (2014) 1236–1257.
[122] X. Cao, et al., Metal oxide-coated three-dimensional graphene prepared by the use of metal-organic frameworks as precursors, Angew. Chem. Int. Ed. Engl. 53 (5) (2014) 1404–1409.
[123] F.H. Shaozhou Li, Metal-organic framework composites: from fundamentals to applications, Nanoscale (2015).
[124] W.W. Zhan, et al., Semiconductor@metal-organic framework core-shell heterostructures: a case of ZnO@ZIF-8 nanorods with selective photoelectrochemical response, J. Am. Chem. Soc. 135 (5) (2013) 1926–1933.
[125] I. Stassen, et al., Solvent-free synthesis of supported ZIF-8 films and patterns through transformation of deposited zinc oxide precursors, CrystEngComm 15 (45) (2013) 9308.
[126] G. Zhang, et al., High-performance and ultra-stable lithium-ion batteries based on MOF-derived ZnO@ZnO quantum dots/C core–shell nanorod arrays on a carbon cloth anode, Adv. Mater. (2015).
[127] P.G. Bruce, et al., Li–O_2 and Li–S batteries with high energy storage, Nat. Mater. 11 (1) (2012) 19–29.
[128] D. Bresser, S. Passerini, B. Scrosati, Recent progress and remaining challenges in sulfur-based lithium secondary batteries—a review, Chem. Commun. 49 (90) (2013) 10545–10562.
[129] A. Manthiram, Y. Fu, Y.S. Su, Challenges and prospects of lithium-sulfur batteries, Acc. Chem. Res. 46 (5) (2013) 1125–1134.
[130] Y.X. Yin, et al., Lithium–sulfur batteries: electrochemistry, materials, and prospects, Angew. Chem. Int. Ed. Engl. 52 (50) (2013) 13186–13200.
[131] S.S. Zhang, Sulfurized carbon: a class of cathode materials for high performance lithium/sulfur batteries, Front. Energy Res. (2013) 1.
[132] J. Scheers, S. Fantini, Johansson, A review of electrolytes for lithium–sulphur batteries, J. Power Sources 255 (2014) 204–218.
[133] R. Demir-Cakan, et al., Cathode composites for Li–S batteries via the use of oxygenated porous architectures, J. Am. Chem. Soc. 133 (40) (2011) 16154–16160.
[134] Z. Wang, et al., A metal–organic framework with open metal sites for enhanced confinement of sulfur and lithium–sulfur battery of long cycling life, Cryst. Growth Des. 13 (11) (2013) 5116–5120.
[135] J. Zheng, et al., Lewis acid–base interactions between polysulfides and metal organic framework in lithium sulfur batteries, Nano Lett. 14 (5) (2014) 2345–2352.
[136] J. Zhou, et al., Rational design of a metal–organic framework host for sulfur storage in fast, long-cycle Li–S batteries, Energy Environ. Sci. 7 (8) (2014) 2715.
[137] J. Zhou, et al., The impact of the particle size of a metal–organic framework for sulfur storage in Li–S batteries, J. Mater. Chem. A 3 (16) (2015) 8272–8275.
[138] B. Liu, et al., Metal-organic framework as a template for porous carbon synthesis, J. Am. Chem. Soc. 130 (16) (2008) 5390–5391.
[139] W. Chaikittisilp, K. Ariga, Y. Yamauchi, A new family of carbon materials: synthesis of MOF-derived nanoporous carbons and their promising applications, J. Mater. Chem. A 1 (1) (2013) 14–19.
[140] X. Han, et al., Reactivation of dissolved polysulfides in Li–S batteries based on atomic layer deposition of Al_2O_3 in nanoporous carbon cloth, Nano Energy 2 (6) (2013) 1197–1206.
[141] G. Xu, et al., Sulfur embedded in metal organic framework-derived hierarchically porous carbon nanoplates for high performance lithium–sulfur battery, J. Mater. Chem. A 1 (14) (2013) 4490.
[142] W. Bao, et al., Multi-walled carbon nanotubes @ mesoporous carbon hybrid nanocomposites from carbonized multi-walled carbon nanotubes @ metal–organic framework for lithium sulfur battery, J. Power Sources 248 (2014) 570–576.
[143] K. Xi, et al., Carbon with hierarchical pores from carbonized metal-organic frameworks for lithium sulphur batteries, Chem. Commun. 49 (22) (2013) 2192–2194.
[144] H.B. Wu, et al., Embedding sulfur in MOF-derived microporous carbon polyhedrons for lithium–sulfur batteries, Chemistry 19 (33) (2013) 10804–10808.
[145] Z. Li, L. Yin, Nitrogen-doped MOF-derived micropores carbon as immobilizer for small sulfur molecules as a cathode for lithium sulfur batteries with excellent electrochemical performance, ACS Appl. Mater. Interfaces 7 (7) (2015) 4029–4038.
[146] X. Li, et al., Tunable porous structure of metal organic framework derived carbon and the application in lithium–sulfur batteries, J. Power Sources 302 (2016) 174–179.
[147] J. Wang, Y. Li, X. Sun, Challenges and opportunities of nanostructured materials for aprotic rechargeable lithium–air batteries, Nano Energy 2 (4) (2013) 443–467.
[148] D. Wu, et al., Metal-organic frameworks as cathode materials for Li–O_2 batteries, Adv. Mater. 26 (20) (2014) 3258–3262.
[149] W. Chen, et al., Hierarchical mesoporous γ-Fe_2O_3/carbon nanocomposites derived from metal organic frameworks as a cathode electrocatalyst for rechargeable Li–O_2 batteries, Electrochim. Acta 134 (2014) 293–301.
[150] J. Zhang, et al., Synthesis of hierarchical porous delta-MnO_2 nanoboxes as an efficient catalyst for rechargeable Li–O_2 batteries, Nanoscale 7 (36) (2015) 14881–14888.
[151] W. Yin, et al., Metal-organic framework derived ZnO/$ZnFe_2O_4$/C nanocages as stable cathode material for reversible lithium–oxygen batteries, ACS Appl. Mater. Interfaces 7 (8) (2015) 4947–4954.
[152] J. Zhang, et al., Porous cobalt-manganese oxide nanocubes derived from metal organic frameworks as a cathode catalyst for rechargeable Li–O_2 batteries, Nanoscale 7 (2) (2015) 720–726.
[153] R. Díaz, et al., Co8-MOF-5 as electrode for supercapacitors, Mater. Lett. 68 (2012) 126–128.
[154] D.Y. Lee, et al., Unusual energy storage and charge retention in Co-based metal–organic-frameworks, Microporous Mesoporous Mater. 153 (2012) 163–165.
[155] D.Y. Lee, et al., Supercapacitive property of metal–organic-frameworks with different pore dimensions and morphology, Microporous Mesoporous Mater. 171 (2013) 53–57.
[156] J. Yang, et al., Metal–organic frameworks: a new promising class of materials for a high performance supercapacitor electrode, J. Mater. Chem. A 2 (39) (2014) 16640–16644.
[157] Y. Tan, et al., Facile synthesis and supercapacitive properties of Zr-metal organic frameworks (UiO-66), RSC Adv. 5 (23) (2015) 17601–17605.
[158] Kyung Min, H.M.J. Choi, Jung Hyo Park, Yue-Biao Zhang, Jeung Ku Kang, Omar M. Yaghi, Supercapacitors of nanocrystalline metal organic frameworks, ACS Nano 8 (2014) 7451–7457.
[159] L. Wang, et al., Flexible solid-state supercapacitor based on a metal-organic framework interwoven by electrochemically-deposited PANI, J. Am. Chem. Soc. 137 (15) (2015) 4920–4923.
[160] H.S. Bo Liu, Akita Tomoki, Qiang Xu, Metal-organic framework as a template for porous carbon synthesis, J. Am. Chem. Soc. 130 (2008) 5390.
[161] B. Liu, et al., Metal–organic framework (MOF) as a template for syntheses of nanoporous carbons as electrode materials for supercapacitor, Carbon 48 (2) (2010) 456–463.
[162] R.R. Salunkhe, et al., Fabrication of symmetric supercapacitors based on MOF-derived nanoporous carbons, J. Mater. Chem. A 2 (46) (2014) 19848–19854.
[163] F. Hao, et al., Synthesis and electrochemical capacitive properties of nitrogen-doped porous carbon micropolyhedra by direct carbonization of zeolitic imidazolate framework-11, Mater. Res. Bull. 66 (2015) 88–95.
[164] S. Zhong, C. Zhan, D. Cao, Zeolitic imidazolate framework-derived nitrogen-doped porous carbons as high performance supercapacitor electrode materials, Carbon 85 (2015) 51–59.
[165] X.Y. Chen, et al., High-performance supercapacitor based on nitrogen-doped porous carbon derived from zinc(II)-bis(8-hydroxyquinoline) coordination polymer, J. Colloid Interface Sci. 393 (2013) 241–248.

[166] W. Chaikittisilp, et al., Nanoporous carbons through direct carbonization of a zeolitic imidazolate framework for supercapacitor electrodes, Chem. Commun. 48 (58) (2012) 7259–7261.
[167] H.L. Jiang, et al., From metal-organic framework to nanoporous carbon: toward a very high surface area and hydrogen uptake, J. Am. Chem. Soc. 133 (31) (2011) 11854–11857.
[168] P. Zhang, et al., ZIF-derived porous carbon: a promising supercapacitor electrode material, J. Mater. Chem. A 2 (32) (2014) 12873.
[169] C. Li, et al., Decoration of graphene network with metal–organic frameworks for enhanced electrochemical capacitive behavior, Carbon 78 (2014) 231–242.
[170] G. Yu, et al., Generation of bimodal porosity via self-extra porogenes in nanoporous carbons for supercapacitor application, J. Mater. Chem. A 2 (37) (2014) 15420.
[171] A.J. Amali, J.K. Sun, Q. Xu, From assembled metal-organic framework nanoparticles to hierarchically porous carbon for electrochemical energy storage, Chem. Commun. (Camb.) 50 (13) (2014) 1519–1522.
[172] J. Tang, et al., Thermal conversion of core–shell metal-organic frameworks: a new method for selectively functionalized nanoporous hybrid carbon, J. Am. Chem. Soc. 137 (4) (2015) 1572–1580.
[173] X.Y. Chen, et al., Structure and electrochemical performance of highly nanoporous carbons from benzoate–metal complexes by a template carbonization method for supercapacitor application, Carbon 72 (2014) 410–420.
[174] X. Yan, et al., Porous carbons prepared by direct carbonization of MOFs for supercapacitors, Appl. Surf. Sci. 308 (2014) 306–310.
[175] Y.-i Fujiwara, et al., Control of pore distribution of porous carbons derived from Mg^{2+} porous coordination polymers, Inorg. Chem. Front. 2 (5) (2015) 473–476.
[176] G. Wang, L. Zhang, J. Zhang, A review of electrode materials for electrochemical supercapacitors, Chem. Soc. Rev. 41 (2) (2012) 797–828.
[177] F.-S. Ke, Y.-S. Wu, H. Deng, Metal-organic frameworks for lithium ion batteries and supercapacitors, J. Solid State Chem. 223 (2015) 109–121.
[178] M. Zhi, et al., Nanostructured carbon–metal oxide composite electrodes for supercapacitors: a review, Nanoscale 5 (1) (2013) 72–88.
[179] F. Meng, et al., Porous Co_3O_4 materials prepared by solid-state thermolysis of a novel Co-MOF crystal and their superior energy storage performances for supercapacitors, J. Mater. Chem. A 1 (24) (2013) 7235.
[180] Y.Z. Zhang, et al., Porous hollow Co(3)O(4) with rhombic dodecahedral structures for high-performance supercapacitors, Nanoscale 6 (23) (2014) 14354–14359.
[181] S. Maiti, A. Pramanik, S. Mahanty, Extraordinarily high pseudocapacitance of metal organic framework derived nanostructured cerium oxide, Chem. Commun. 50 (79) (2014) 11717–11720.
[182] S. Chen, et al., Porous ZnCo2O4 nanoparticles derived from a new mixed-metal organic framework for supercapacitors, Inorg. Chem. Front. 2 (2) (2015) 177–183.
[183] I.A. Khan, et al., A copper based metal-organic framework as single source for the synthesis of electrode materials for high-performance supercapacitors and glucose sensing applications, Int. J. Hydrog. Energy 39 (34) (2014) 19609–19620.
[184] W. Meng, et al., Porous Fe_3O_4/carbon composite electrode material prepared from metal-organic framework template and effect of temperature on its capacitance, Nano Energy 8 (2014) 133–140.
[185] M.-S. Wu, W.-H. Hsu, Nickel nanoparticles embedded in partially graphitic porous carbon fabricated by direct carbonization of nickel-organic framework for high-performance supercapacitors, J. Power Sources 274 (2015) 1055–1062.
[186] S. Ullah, et al., A novel Cr_2O_3-carbon composite as a high performance pseudo-capacitor electrode material, Electrochim. Acta 171 (2015) 142–149.
[187] R. Wu, et al., MOF-derived copper sulfides embedded within porous carbon octahedra for electrochemical capacitor applications, Chem. Commun. 51 (15) (2015) 3109–3112.
[188] X.Y. Yu, et al., Formation of nickel sulfide nanoframes from metal-organic frameworks with enhanced pseudocapacitive and electrocatalytic properties, Angew. Chem. Int. Ed. Engl. 54 (18) (2015) 5331–5335.
[189] L.Q. Mai, et al., Hierarchical MnMoO(4)/CoMoO(4) heterostructured nanowires with enhanced supercapacitor performance, Nat. Commun. 2 (2011) 381.
[190] J. Bae, et al., Fiber supercapacitors made of nanowire-fiber hybrid structures for wearable/flexible energy storage, Angew. Chem. Int. Ed. Engl. 50 (7) (2011) 1683–1687.
[191] Z. Jiang, et al., LDH nanocages synthesized with MOF templates and their high performance as supercapacitors, Nanoscale 5 (23) (2013) 11770–11775.
[192] H. Hu, et al., Designed formation of Co_3O_4/$NiCo_2O_4$ double-shelled nanocages with enhanced pseudocapacitive and electrocatalytic properties, J. Am. Chem. Soc. 137 (16) (2015) 5590–5595.